Late spring bloom development of pelagic diatoms in Baffin Bay

Augustin Lafond, Karine Leblanc, Bernard Queguiner, Brivaëla Moriceau, Aude Leynaert, Veronique Cornet, Justine Legras, Joséphine Ras, Marie Parenteau, Nicole Garcia, et al.

Late spring bloom development of pelagic diatoms in Baffin Bay

Article · November 2019

CITATIONS
0

READS
2

10 authors, including:

Augustin Lafond
Aix-Marseille Université
4 PUBLICATIONS **0** CITATIONS
SEE PROFILE

Karine Leblanc
Aix-Marseille Université
90 PUBLICATIONS **2,514** CITATIONS
SEE PROFILE

Bernard Quéguiner
Institut Méditerranéen d'océanologie
175 PUBLICATIONS **6,319** CITATIONS
SEE PROFILE

Brivaela Moriceau
Université de Bretagne Occidentale
43 PUBLICATIONS **899** CITATIONS
SEE PROFILE

ELEMENTA
Science of the Anthropocene

Lafond, A, et al. 2019. Late spring bloom development of pelagic diatoms in Baffin Bay. *Elem Sci Anth,* 7: 44. DOI: https://doi.org/10.1525/elementa.382

RESEARCH ARTICLE

Late spring bloom development of pelagic diatoms in Baffin Bay

Augustin Lafond[*], Karine Leblanc[*], Bernard Quéguiner[*], Brivaela Moriceau[†], Aude Leynaert[†], Véronique Cornet[*], Justine Legras[*], Joséphine Ras[‖], Marie Parenteau[‡,§], Nicole Garcia[*], Marcel Babin[‡,§] and Jean-Éric Tremblay[‡,§]

The Arctic Ocean is particularly affected by climate change, with changes in sea ice cover expected to impact phytoplankton primary production. During the Green Edge expedition, the development of the late spring–early summer diatom bloom was studied in relation with the sea ice retreat by multiple transects across the marginal ice zone. Biogenic silica concentrations and uptake rates were measured. In addition, diatom assemblage structures and their associated carbon biomass were determined, along with taxon-specific contributions to total biogenic silica production using the fluorescent dye PDMPO. Results indicate that a diatom bloom developed in open waters close to the ice edge, following the alleviation of light limitation, and extended 20–30 km underneath the ice pack. This actively growing diatom bloom (up to 0.19 µmol Si L^{-1} d^{-1}) was associated with high biogenic silica concentrations (up to 2.15 µmol L^{-1}), and was dominated by colonial fast-growing centric (*Chaetoceros* spp. and *Thalassiosira* spp.) and ribbon-forming pennate species (*Fragilariopsis* spp./*Fossula arctica*). The bloom remained concentrated over the shallow Greenland shelf and slope, in Atlantic-influenced waters, and weakened as it moved westwards toward ice-free Pacific-influenced waters. The development resulted in a near depletion of all nutrients eastwards of the bay, which probably induced the formation of resting spores of *Melosira arctica*. In contrast, under the ice pack, nutrients had not yet been consumed. Biogenic silica and uptake rates were still low (respectively <0.5 µmol L^{-1} and <0.05 µmol L^{-1} d^{-1}), although elevated specific Si uptake rates (up to 0.23 d^{-1}) probably reflected early stages of the bloom. These diatoms were dominated by pennate species (*Pseudo-nitzschia* spp., *Ceratoneis closterium*, and *Fragilariopsis* spp./*Fossula arctica*). This study can contribute to predictions of the future response of Arctic diatoms in the context of climate change.

Keywords: Diatoms; Spring bloom; Sea ice; Community composition; Baffin Bay; Arctic

Introduction

Arctic marine ecosystems are currently undergoing multiple environmental changes in relation with climate change (ACIA, 2005; IPCC, 2007; Wassmann et al., 2011). The perennial sea ice extent has dropped by approximately 9% per decade since the end of the 1970s (Comiso, 2002), and models predict an ice-free summer in the Arctic during the course of this century (Stroeve et al., 2007; Wang and Overland, 2009). In addition, the multiyear sea ice is progressively being replaced by thinner first year ice (Kwok et al., 2009; Maslanik et al., 2011), the annual phytoplankton bloom is occurring earlier (Kahru et al., 2011), and the duration of the open water season is extending (Arrigo and van Dijken, 2011). The result has been an increasing amount of light penetrating the ocean surface, thus increasing the habitat suitable for phytoplankton growth. Based on satellite data, some studies have highlighted that the total annual net primary production is already increasing in the Arctic Ocean, between 14–20% over the 1998–2010 period (Arrigo et al., 2008; Pabi et al., 2008; Arrigo and van Dijken, 2011; Bélanger et al., 2013). Ardyna et al. (2014) have also revealed that some Arctic regions are now developing a second phytoplankton bloom during the fall, due to delayed freeze-up and increased exposure of the sea surface to wind stress.

However, models do not agree on the future response of marine primary production to these alterations (Steinacher et al., 2010; Vancoppenolle et al., 2013).

* Aix-Marseille University, Université de Toulon, CNRS, IRD, MIO, UM 110, 13288, Marseille FR

† Laboratoire des Sciences de l'Environnement Marin, Institut Universitaire Européen de la Mer, Technopole Brest-Iroise, Plouzané, FR

‡ Takuvik Joint International Laboratory, Laval University (Canada), CNRS, FR

§ Département de biologie et Québec-Océan, Université Laval, Québec, CA

‖ Sorbonne Universités, UPMC Univ Paris 06, CNRS, IMEV, Laboratoire d'Océanographie de Villefranche, Villefranche-sur-mer, FR

Corresponding author: Augustin Lafond (augustin.lafond@gmail.com)

Although a correlation between annual primary production and the length of the growing season has been demonstrated (Rysgaard et al., 1999; Arrigo and van Dijken, 2011), Tremblay and Gagnon (2009) proposed that the production should lessen in the future due to dissolved inorganic nitrogen limitation, unless the future physical regime promotes recurrent nutrient renewal in the surface layer. Future nutrient trends are likely to vary considerably across Arctic regions. While fresher waters in the Beaufort Gyre may lead to increased stratification and nutrient limitation (Wang et al., 2018), the northern Barents Sea may soon complete the transition from a cold and stratified Arctic to a warm and well-mixed Atlantic-dominated climate regime (Lind et al., 2018). Another consequence of the ongoing changes in Arctic sea ice is the intrusion of Atlantic and Pacific phytoplankton species into the high Arctic (Hegseth and Sundfjord, 2008). One of the most prominent examples is the cross-basin exchange of the diatom *Neodenticula seminae* between the Pacific and the Atlantic basins for the first time in 800,000 years (Reid et al., 2007).

In seasonally ice-covered areas, spring blooms occur mostly at the ice edge, forming a band moving northward as the ice breaks up and melts over spring and summer (Sakshaug and Skjoldal, 1989; Perrette et al., 2011). As the sea ice melts at the ice edge, more light enters the newly exposed waters, and the water column becomes strongly stratified due to freshwater input, creating the necessary stability for phytoplankton to grow. Spring blooms are responsible for a large part of the annual primary production in marine Arctic ecosystems (Sakshaug, 2004; Perrette et al., 2011), provide energy to marine food webs, and play a major role in carbon sequestration and export (Wassmann et al., 2008). Although they often co-occur with the haptophyte *Phaeocystis pouchetii*, diatoms have been described as the dominant phytoplankton group during Arctic spring blooms at many locations including northern Norway (Degerlund and Eilertsen, 2010), the central Barents Sea (Wassmann et al., 1999), the Svalbard Archipelago (Hodal et al., 2012), the Chukchi Sea (Laney and Sosik, 2014), and the North Water polynya (Lovejoy et al., 2002). However, due to logistical challenges, spring bloom dynamics in the Arctic have rarely been studied.

Baffin Bay is almost completely covered by ice from December to May. In the centre of the bay, the ice edge retreats evenly westward from Greenland towards Nunavut (Canada) and features a predictable spring bloom (Perrette et al., 2011; Randelhoff et al., 2019). In addition, Baffin Bay is characterized by a west–east gradient in water masses: the warm and salty Atlantic-derived waters enter Baffin Bay from the eastern side of the Davis Strait and are cooled as they circulate counter-clockwise within the bay by the cold and fresh Arctic waters entering from the northern Smith, Jones and Lancaster Sounds (Tremblay, 2002; Tang et al., 2004). Baffin Bay is thus a good model to study both the role played by water masses and the sea ice cover in the development of diatoms during the spring bloom.

The aim of this work was to study, for the first time in central Baffin Bay, the development of the late spring–early summer diatom bloom in relation with the retreat of the pack ice. The following questions are addressed: What are the factors that control the onset, maintenance and end of the diatom bloom around the ice edge, under the ice pack and in adjacent open waters? What are the key diatom species involved during the bloom, in terms of abundance, carbon biomass and silica uptake activities? What are the functional traits that enable these species to thrive in these waters?

Materials and Methods

Study area and sampling strategy

The Green Edge expedition was carried out in Baffin Bay aboard the research icebreaker NGCC *Amundsen* from 3 June to 14 July 2016 (**Figure 1**). Baffin Bay is characterized by a large abyssal plain in the central region (with depths

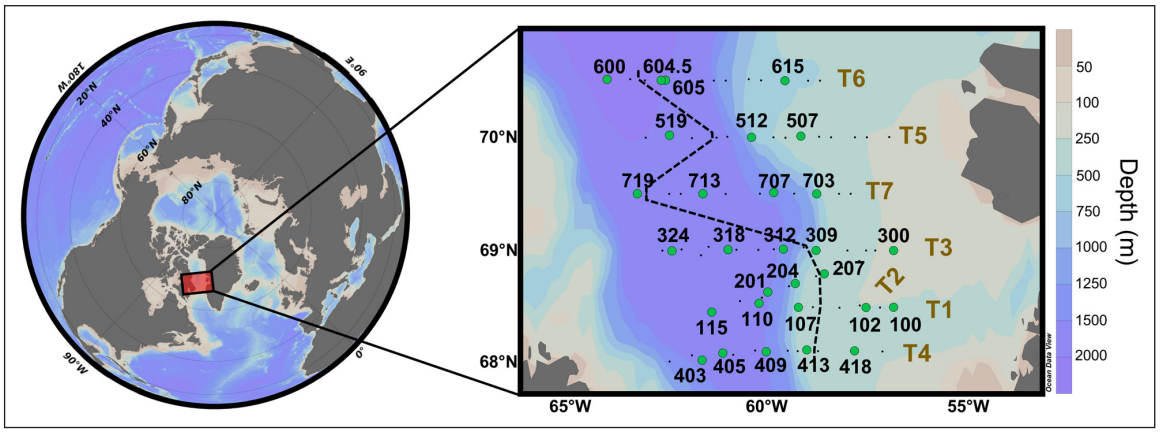

Figure 1: Location of the sampling stations during the Green Edge expedition. Hydrology, nutrients, and pigment analysis were performed at all stations (black dots and green circles). The silicon cycle was studied at stations indicated by green circles. Transects T1 to T7 are numbered following their chronological order of sampling. Transects were sampled during the following periods: T1, 9–13 June; T2, 14–17 June; T3, 17–22 June; T4, 24–29 June; T5, 29 June–3 July; T6, 3–7 July; T7, 7–10 July. The black dashed line represents the approximate location of the ice edge at the time of sampling of each transect. Stations located west of this line were covered by sea ice when sampled. DOI: https://doi.org/10.1525/elementa.382.f1

to 2300 m) and continental shelves located on both sides of the bay. The continental shelf off Greenland is wider and ends with an abrupt shelf break. The icebreaker performed seven perpendicular transects across the marginal ice zone (MIZ) from the open waters to the sea ice, covering an area from 67°N to 71°N, and from 55°W to 64°W. This sampling strategy was chosen in order to capture every step of the bloom phenology: from a pre-bloom situation under the compact sea ice at the western ends of transects, through the bloom initiation and growth close to the ice edge, to a post-bloom situation at the easternmost open water stations. The number assigned to each transect (T1 to T7) follows the chronological order of sampling. This order was dictated by the optimization of the ship's route, which was constrained by a mid-cruise changing of the scientific team and sea ice conditions.

Sample collection and analyses

Hydrographic data

At each hydrographic station, seawater collection and vertical profiles of water column properties were made from an array of 24, 12-L bottles mounted on a rosette equipped with a Seabird SBE-911 plus CTD unit, which also included a Seapoint SCF Fluorometer for detection of chlorophyll *a* (Chl *a*). Close to the rapidly melting marginal ice zone, density profiles often did not exhibit a well-mixed layer nor a clear density step below; hence we calculated an equivalent mixed layer (hBD) as defined in Randelhoff et al. (2017), used for strongly meltwater-influenced layers in the marginal ice zone (MIZ). Also in accordance with Randelhoff et al. (2019), we defined the depth of the euphotic zone (Ze) as the depth where a daily irradiance of photosynthetically available radiation (PAR) of 0.415 Einstein m^{-2} d^{-1} was measured. This value delimits the lower extent of the vertical phytoplankton distribution in the north Pacific subtropical gyre (Letelier et al., 2004). Based on Green Edge data, Randelhoff et al. (2019) showed that Ze estimated using the 0.415 Einstein m^{-2} d^{-1} criteria was not statistically different from Ze estimated using the more widely-used 1% surface PAR criteria. Vertical profiles of instantaneous downwelling irradiance were measured to a depth of 100 m using a Compact Optical Profiling System (C-OPS, Biospherical Instruments, Inc.). Daily PAR just above the sea surface was estimated using both in situ data recorded on the ship's meteorological tower and the atmospheric radiative transfer model SBDART (Ricchiazzi et al., 1998). More information about light transmittance in the water column and its measurement methodology (in particular for sea ice-covered stations) can be found in Randelhoff et al. (2019).

Dissolved nutrients

Nutrient (NO_3^-, PO_4^{3-}, H_4SiO_4) analyses were performed onboard on a Bran+Luebbe Autoanalyzer 3 using standard colorimetric methods (Grasshoff et al., 2009). Analytical detection limits were 0.03 µmol L^{-1} for NO_3^-, 0.05 µmol L^{-1} for PO_4^{3-} and 0.1 µmol L^{-1} for H_4SiO_4.

The Atlantic and Pacific Oceans provide source waters for the Arctic Ocean that can be distinguished by their differing nitrate and phosphate concentration relationship. Following Jones et al. (1998), the 'Arctic N-P' tracer (ANP) was calculated for each station. It quantifies the proportion of Atlantic and Pacific waters in a water body using their N-P signatures. Essentially, ANP = 0% means the NO_3^-/PO_4^{3-} pairs fall on the regression line for Atlantic waters, whereas ANP = 100% means the NO_3^-/PO_4^{3-} pairs fall on the regression line for Pacific waters. Because the ANP index is a ratio, it is a quasi-conservative water mass tracer and is not influenced by the biological consumption of nutrients. The limit between 'Pacific' vs 'Atlantic' influenced waters was placed arbitrarily at stations where the ANP = 25%.

Pigments

For pigment measurements, <2.7 L seawater samples were filtered on Whatman GF/F filters and stored in liquid nitrogen until analysis. Back at the laboratory, all samples were analyzed within three months. Filters were extracted in 100% methanol, disrupted by sonication, and clarified by filtration (GF/F Whatman) after 2 h. Samples were analysed within 24 h using High Performance Liquid Chromatography on an Agilent Technologies HPLC 1200 system equipped with a diode array detector following Ras et al. (2008).

Sea ice satellite data

Sea ice concentrations (SIC) have been extracted from AMSR2 radiometer daily data on a 3.125 km grid (Beitsch et al., 2014). At each station, the SIC was extracted from the closest pixel using the Euclidian distance between the ship position and the centre of each pixel. The SIC is an index that ranges between 0 (complete open water) and 1 (complete ice cover). Here, we placed the ice-edge limit at stations with SIC = 0.5. Based on SIC history, we also retrieved the number of days between the sampling day and the day at which SIC dropped below 0.5 (DOW50) to estimate the timing of the melting of sea ice. DOW50 can take positive or negative values, depending if SIC at the time of sampling is >0.5 (DOW50 negative) or <0.5 (DOW50 positive).

Description of the diatom bloom

Particulate silica concentrations

Biogenic (BSi) and lithogenic (LSi) silica concentrations were measured at 29 stations covering the seven transects (**Figure 1**). Samples were taken at 7 to 14 depths between 0 and 1674 m depth. For each sample, 1 L of seawater was filtered onto 0.4 µm Nucleopore polycarbonate filters. Filters were then stored in Eppendorf vials, and dried for 24 h at 60°C before being stored at room temperature. Back at the laboratory, BSi was measured by the hot NaOH digestion method of Paasche (1973) modified by Nelson et al. (1989). After NaOH extraction, filters were assayed for LSi by HF addition for 48 h using the same filter.

Biogenic silica uptake rates (ρSi)

Biogenic Si uptake rates (ρSi) were measured by the ^{32}Si method (Tréguer et al., 1991; Brzezinski and Phillips, 1997) for 21 stations at 5 to 7 different depths, corresponding to different levels of PAR, ranging from 75 to 0.1% of surface irradiance. At the ice-covered stations, samples that were collected under the ice were incubated

in the same way as the samples collected in open waters, because onboard we only had access to the light transmittance through the water column that did not take into account attenuation through the ice. However, at three stations (201, 403, and 409) we were able to perform two incubation experiments in parallel that either did or did not take into account the light attenuation through the ice. Due to light attenuation at depth, this affects only the first 20 m where we have estimated a mean bias in our ρSi measurement under the ice of 0.005 ± 0.003 μmol L^{-1} d^{-1} (i.e. 23 ± 9% difference), which should not change substantially the interpretation of the main results, but would have to be taken into account if our data are used to constrain a regional Si budget.

The following equation was used to calculate Si uptake rates:

$$\rho Si = Af \times \frac{[H_4SiO_4]}{Ai} \times \frac{24}{T}$$

where *Af* is the final activity of the sample, *Ai* the initial activity, and *T* the incubation time (in hours). Briefly, polycarbonate bottles filled with 160 mL of seawater were spiked with 667 Bq of radiolabeled ^{32}Si-silicic acid solution (specific activity of 18.5 kBq μg-Si^{-1}). For most of the samples, H_4SiO_4 addition did not exceed 1% of the initial concentration. Samples were then placed in a deck incubator cooled by running sea surface water and fitted with blue plastic optical filters to simulate the light attenuation of the corresponding sampling depth. After 24 h, samples were filtered onto 0.6 μm Nucleopore polycarbonate filters and stored in a scintillation vial until further laboratory analyses. ^{32}Si activity on filters was measured in a Packard 1600 TR scintillation counter by Cerenkov counting following Tréguer et al. (1991). The background for the ^{32}Si radioactive activity counting was 10 cpm. Samples for which the measured activity was less than 3 times the background were considered to lack Si uptake activity. The specific Si uptake rate VSi (d^{-1}) was calculated by normalizing ρSi by BSi.

Taxon-specific contribution to biogenic silica production (PDMPO)

Taxon-specific silica production was quantified using the fluorescent dye PDMPO, following Leblanc and Hutchins (2005), which allows quantification of newly deposited Si at the specific level in epifluorescence microscopy. Compared to confocal microscopy, this technique allows analysis of a large number of cells and therefore gives a robust estimation of the activity per taxon. Although images are acquired in two dimensions, superimposed fluorescence in the vertical plane increases the fluorescence in the x–y plane and reduces measurement biases. Briefly, 170 mL of seawater samples were spiked onboard with 0.125 μmol L^{-1} PDMPO (final concentration) and incubated in the deck incubator for 24 h. The samples were then centrifuged down to a volume of 2 mL, resuspended with 10 mL methanol, and then kept at 4°C. At the laboratory, samples were mounted onto permanent glass slides and stored at –20°C before analysis. Microscope slides were then observed under a fluorescence inverted microscope Zeiss Axio Observer Z1 equipped with a Xcite 120LED source and a CDD black and white AxioCam-506 Mono (6 megapixel) camera fitted with a filter cube (Ex: 350/50; BS 400 LP; Em: 535/50). Images were acquired sequentially in bright field and epifluorescence, in order to improve species identification for labelled cells. PDMPO fluorescence intensity was quantified for each taxon following Leblanc and Hutchins (2005) using a custom-made IMAGE J routine on original TIFF images. The taxon-specific contributions to silica production were estimated by multiplying, for each taxon, the number of fluorescent cells by the mean fluorescence per cell.

Diatom identification and counting

Seawater samples collected with the rosette at discrete depths were used for diatom identification and quantitative assessment of diatom assemblages. Prior to counting, diatom diversity was investigated at three stations using a Phenom Pro scanning electron microscope (SEM) (See Figure S1 for SEM pictures illustrating the key species). For SEM analysis, water samples were filtered (0.25–0.5 L) onto polycarbonate filters (0.8 μm pore size, Whatman), rinsed with trace ammonium solution (pH 10) to remove salt water, oven-dried (60°C, 10 h) and stored in Millipore PetriSlides. Pictures were taken at magnification up to × 25,000.

Cell counts were done within a year after the expedition. Samples were regularly checked and lugol was added when needed. In total, 43 samples were analysed from 25 stations (**Figure 1**): 23 were collected at the near surface (0–2 m depth), and 20 were collected at the depth of the subsurface chlorophyll *a* maximum (SCM) when the maximum of Chl *a* was not located at the surface. Aliquots of 125 mL were preserved with 0.8 mL acidified Lugol's solution in amber glass bottles, then stored in the dark at 4°C until analysis. Counting was performed in the laboratory following Utermöhl (1931) using a Nikon Eclipse TS100 inverted microscope. For counting purposes, minimum requirements were to count at least three transects (length: 26 mm) at ×400 magnification and at least 400 planktonic cells (including Bacillariophyceae, but also Dinophyceae, flagellates, and ciliates). Raw counts were then converted to number of cells per litre. In this paper, only data on diatom counting are presented.

Conversion to carbon biomass

Diatom-specific C biomass was assessed following the methodology of Cornet-Barthaux et al. (2007). Except for rare species, cell dimensions were determined from representative images of each of 35 taxa, where the mean (± standard deviation) number of cells measured per taxon was 21 (±14) (see Table S1). Measuring the three dimensions of the same cell is usually difficult. When not visible, the third dimension was estimated from dimension ratios documented in European standards (BS EN 16695, 2015). For each measured cell, a biovolume was estimated using linear dimensions in the appropriate geometric formula reflecting the cell shape (BS EN 16695, 2015). A mean biovolume was then estimated for each taxon and converted

to carbon content per cell according to the corrected equation of Eppley (Smayda, 1978), as follows:

$$\text{Log C biomass} = 0.76\ \text{Log}\ (\text{cell volume}) - 0.352$$

C content per cell (pg cell^{-1}) was multiplied by cell abundance (cells L^{-1}) to derive total carbon biomass per taxon, expressed in units of µg C L^{-1}.

Statistical analyses

Diatom assemblage structures were investigated through cluster analysis (Legendre and Legendre, 2012). Abundance data were normalized by performing a Log (x + 1) transformation. Euclidean distances were then calculated between each pair of samples, and the cluster analysis was performed on the distance matrix using Ward's method (1963). Cluster analysis based on Bray-Curtis similarities gave the same clusters. The output dendrogram displays the similarity relationship among samples. An arbitrary threshold was applied to separate samples into compact clusters. A post hoc analysis of similarity (one-way ANOSIM) was performed to determine whether clusters differed statistically from each other in terms of taxonomic composition.

Trait-based analysis

A trait-based analysis was performed following Fragoso et al. (2018) to identify functional traits that determine species ecological niches (data used are listed in Table S2). Briefly, eight diatom traits were selected according to their ecological relevance and availability of information in the literature: equivalent spherical diameter (ESD); surface area to volume ratio (S/V); optimum temperature for growth (T_{opt}); ability to produce ice-binding proteins (IBP); the presence or absence of long, sharp projections such as setae, spines, horns and cellular processes (spikes); degree of silicification, qualitatively based on examination of SEM images (silicified); the propensity to form resting spores (spores); and the ability to form colonies (colonies). More detailed description of the traits can be found in Fragoso et al. (2018). Due to the difficulty of finding information about every trait for every diatom species, only the dominant taxa were included in the analysis and some species were grouped on the basis of trait similarities. A community-weighted trait mean (CWM) is an index used to estimate trait variability on a community level. CWM values were calculated for each trait in each sample from two matrices: a matrix that gives trait values for each species, and a matrix that gives the relative abundances for each species in each sample. CWM is calculated according to the following equation:

$$\text{CWM} = \sum_{i=1}^{S} p_i . x_i$$

where S is the number of species in the assemblage, p_i is the relative abundance of each species, and x_i is the species-specific trait value. Each of the eight traits was normalized in relation to the stations that presented the lowest (= 0) and the highest values (=1).

Results

Environmental conditions

Ice cover and water masses

As shown in **Figure 2a, b** depicting sea ice concentrations, the expedition was marked by the westward retreat of the sea ice in Baffin Bay (all data and metadata are summarized in Table S3). Just before the beginning of the

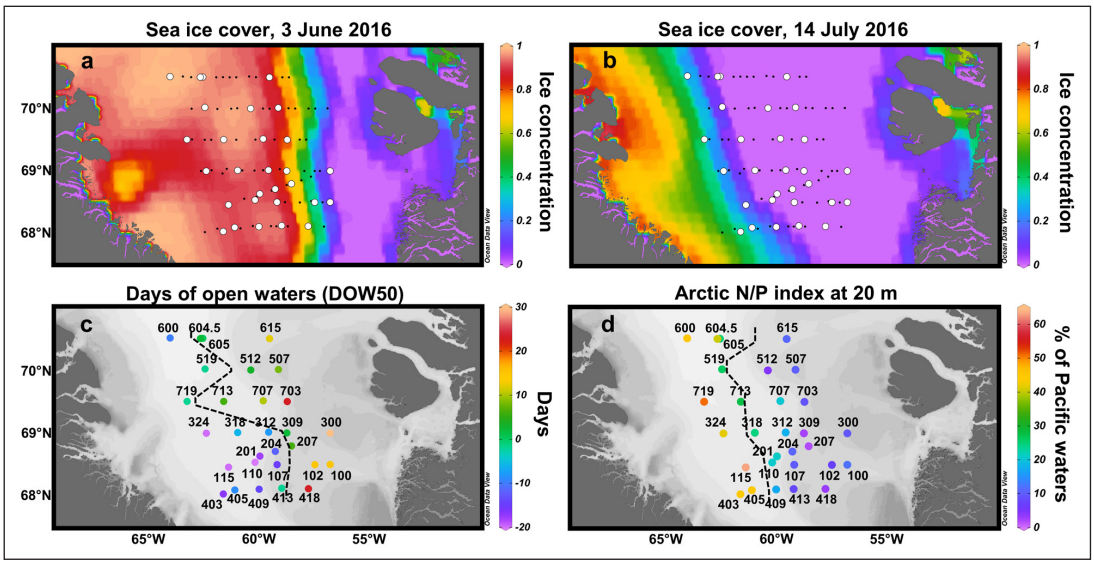

Figure 2: Hydrographic conditions in central Baffin Bay during June–July 2016. (a–b) Five-day composite images of sea ice concentrations. White circles correspond to the stations where the silicon cycle was studied. **(c)** Number of days since the sea ice concentration dropped below 0.5 (DOW50). The black dashed line corresponds to the approximate location of the ide edge at the time of sampling (i.e., where DOW50 = 0). **(d)** Fraction of Pacific waters at 20 m (ANP index). The black dashed line delimits the Pacific-influenced waters (ANP > 25%) from the Atlantic-influenced waters (ANP < 25%). DOI: https://doi.org/10.1525/elementa.382.f2

expedition (3 June), most of the stations where the silicon cycle was studied were covered by sea ice, whereas at the end of the expedition (14 July), all were ice-free, with the exception of station (st.) 719. A composite picture of DOW50 at each site at the time of sampling is presented in **Figure 2c**. The retreat of the melting sea ice towards the west was more pronounced during the last three transects (T5–T7) as shown by the ice-edge position (located where DOW50 = 0 and SIC = 0.5). West of this limit, stations were covered by sea ice (SIC > 0.5) when sampled, whereas to the east, the sea ice had already melted (SIC <0.5) since a number of days ranging from 0 (st. 605) to 31 (st. 300).

Using the Arctic N-P relationship calculated from nutrient samples collected at 20-m depth, the fraction of Pacific waters in the water samples increased westwards (**Figure 2d**), in accordance with the global circulation pattern established for Baffin Bay. Most of the eastern stations exhibited an ANP <15%, whereas ANP increased significantly from the middle of the bay to the westernmost stations, reaching 63% at st. 115. Atlantic- and Pacific-influenced waters (delimited by ANP = 25%) were also associated with wide differences in salinity, temperature and density profiles in the upper layer (Figure S2). According to Tang et al. (2004), these wide differences are due to the warm and salty inflow of the West Greenland Current from the eastern side of Davis Strait (entailing Atlantic-influenced waters to the east) and the cold and fresh outflow from the Canadian Archipelago and water masses produced within Baffin Bay (entailing Pacific-influenced waters to the west). The warm current along the west coast of Greenland also explains why the sea ice melts toward the west in Baffin Bay (Tang et al., 2004), whereas in the other Arctic regions, it usually melts northward (Perrette et al., 2011).

Nutrient distribution

The distribution of nutrients (**Figure 3**) in surface waters was characterized by a decreasing west-to-east gradient that generally followed the ice coverage at the time of sampling. Overall, surface concentrations were higher at stations covered by sea ice (maximum concentrations: $[H_4SiO_4] = 9.2$ µmol L^{-1}; $[NO_3^-] = 5.9$ µmol L^{-1}; $[PO_4^{3-}] = 0.9$ µmol L^{-1}). In contrast, at open-water stations located east of the ice edge, nutrients were close to exhaustion, some-

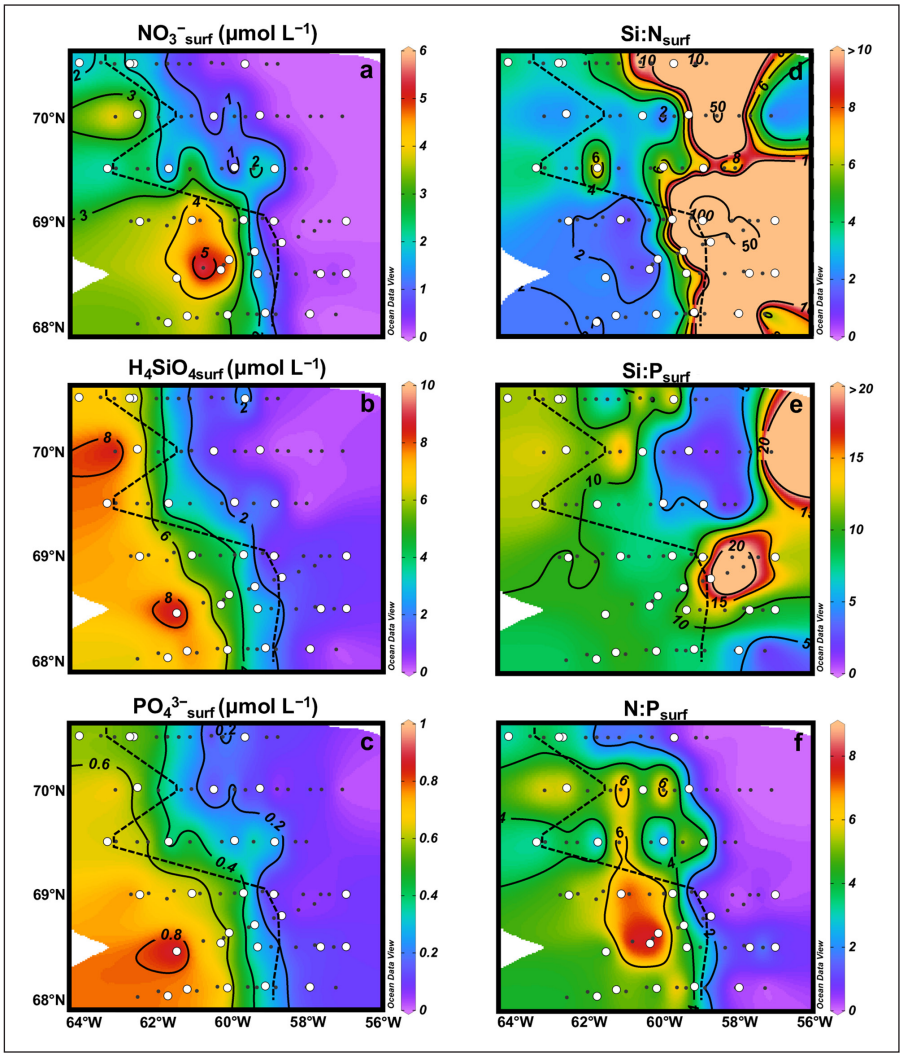

Figure 3: Surface nutrient concentrations and potential limiting nutrients. Concentrations of surface nitrate **(a)**, orthosilicic acid **(b)**, and phosphate **(c)** in µmol L^{-1}. Molar ratios of Si:N **(d)**, Si:P **(e)**, and N:P **(f)** at the surface. The black dashed lines correspond to the approximate location of the ice edge. The white circles correspond to the stations where the silicon cycle was studied. DOI: https://doi.org/10.1525/elementa.382.f3

times near detection limits ($0 < [H_4SiO_4] < 1.4$ µmol L^{-1}; $0 < [NO_3^-] < 0.7$ µmol L^{-1}; $0 < [PO_4^{3-}] < 0.2$ µmol L^{-1}), except for stations 605 and 604.5 where nutrient concentrations were similar to the ice-covered stations. For the southern transects (T1–T4) and T5, nutrient depletion extended well inside the ice pack. The vertical distribution of nutrients along transects (Figure S3) indicated that depletion extended to greater depths towards the east, especially for orthosilicic acid which was depleted down to 60-m depth. The west-east gradient observed at the surface was also found when nutrients were integrated over the depth of the equivalent mixed layer (Supplemental Figure S4).

The nutrient ratios Si:N:P = 16:16:1 derived from Redfield et al. (1963) and Brzezinski (1985) can be used to determine the potential limiting nutrients for diatoms. Overall, in surface waters (**Figure 3d–f**) and down to 20–30 m (Figure S5), Si:N > 1, Si:P < 16 (except on the eastern part of T2, T3 and T5) and N:P < 16, indicating that NO_3^- was the first potentially limiting nutrient, followed by H_4SiO_4 and PO_4^{3-}. Nitrate limitation (**Figure 3d**) was much more pronounced in the eastern half of the bay because nitrate concentrations were close to zero. At 40-m depth (Figure S5), Si:N was generally lower than 1 on the eastern side of the bay, indicating a potential silicic acid limitation in those subsurface waters.

Integrated proxies of protist biomass

The TChl *a* standing stock, an indicator of algal biomass, was integrated over 80-m depth (**Figure 4a**). Values were highest at st. 615 (164.4 mg m^{-2}; up to 12.8 µg L^{-1} at 26 m), in the northeast of the sampling area. High values were also observed in the eastern parts of T1–T3 (between 44.3 and 100.7 mg m^{-2}; up to 3.5 µg L^{-1} at st. 207 at 15 m), and in the middle of T5–T7 (>71.9 mg m^{-2}; up to 9.6 µg L^{-1} at st. 512 at 20 m). Integrated TChl *a* was lower in the rest of the studied area (between 5.5 and 48.0 mg m^{-2}), especially on the western side and throughout T4. Vertical sections (Figure S3) show that the TChl *a* distribution was mainly located within the subsurface maximum that deepened to 60-m depth at the easternmost stations, characterizing late bloom conditions.

The chlorophyll-c_3 (Chl c_3) pigment was used as a diagnostic pigment for *Phaeocystis* spp. biomass instead of the more traditionally used 19′Hexanoyloxyfucoxanthin, as the latter has been shown to be absent in arctic *Phaeocystis* strains (Antajan et al., 2004; Stuart et al., 2000). A significant linear relationship ($R^2 = 0.74$; $p < 0.0001$; $n = 36$) was obtained between Chl c_3 concentrations (in µg L^{-1}) and *Phaeocystis* spp. abundances determined by microscopic counts (Figure S6). When integrated over 80-m depth (**Figure 4b**), the highest Chl c_3 standing stock was

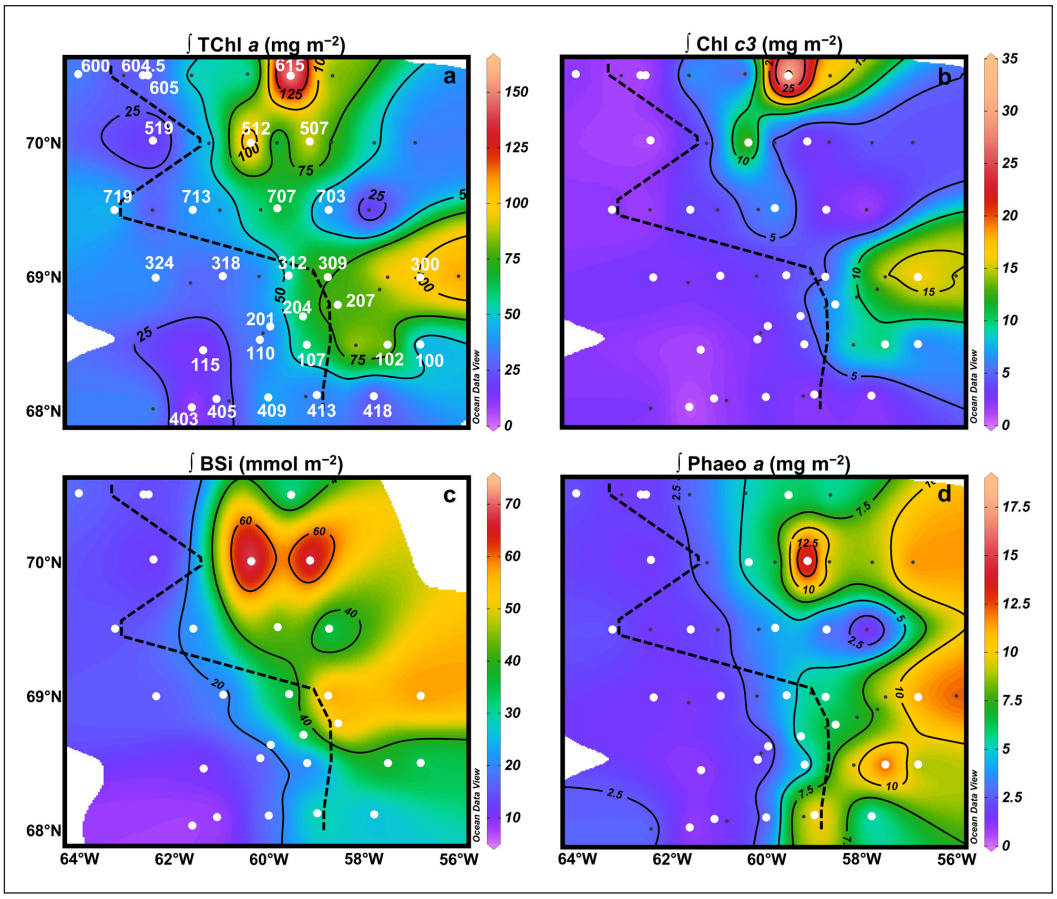

Figure 4: Depth-integrated phytoplankton pigments and BSi throughout the study area. Distribution of depth-integrated TChl *a* **(a)**, Chl c_3 **(b)**, BSi **(c)**, and Phaeophorbide *a* **(d)**. Vertical integrations were made from the surface to 80 m, because at that depth almost all Chl *a* profiles were sufficiently close to 0, indicating that no significant biomass was missed. The black dashed lines correspond to the approximate location of the ice edge at the time of sampling. White circles indicate the stations where the silicon cycle was studied. Integrated pigments (a, b and d) are expressed in mg m^{-2} and BSi (c) in mmol m^{-2}. DOI: https://doi.org/10.1525/elementa.382.f4

observed at st. 615 (35.5 mg m^{-2}) and matched the subsurface Chl *a* peak. High amounts of Chl c_3 were also found at st. 512 (16.9 mg m^{-2}) and 300 (17.4 mg m^{-2}). At these stations (except for st. 512), the Chl c_3:TChl *a* ratio reached values equal to or slightly higher than 0.20 (up to 0.23), which is typical of *Phaeocystis* species (Antajan et al., 2004; Stuart et al., 2000).

At st. 615, integrated BSi over 80-m depth (**Figure 4c**) was low (27.2 mmol m^{-2}) compared to the other stations located east of the ice edge. Throughout the area, two BSi accumulation areas were observed, located at stations 507 and 512 (reaching 79.6 mmol m^{-2}) and at stations 207, 300, 309 (reaching 63.4 mmol m^{-2}) (see next section for details of vertical distribution).

Phaeophorbide *a* is a degradation product of Chl *a* (**Figure 4d**) and is indicative of grazing. When integrated over 80-m depth, low standing stocks were observed throughout section T7 and at the western sea ice-covered stations (<4.4 mg m^{-2}), except for stations located close to the ice edge on sections T1–T4. Along these transects, moderate to high phaeophorbide *a* standing stocks (>4.5 mg m^{-2}) were measured from right below the ice edge to the end of the transect to the east, with maximum values at st. 102 (14.3 mg m^{-2}) and st. 413 (11.6 mg m^{-2}). For sections T5 and T6, standing stocks started to increase far from the ice edge, with a maximum throughout the studied area observed at st. 507 (18.9 mg m^{-2}).

Vertical distribution of particulate silica and BSi uptake rates

Particulate silica concentrations

Throughout the study area, very low BSi concentrations (<0.49 µmol L^{-1}) were observed at stations covered by sea ice (**Figure 5**), except for a few stations located close to the ice edge (e.g. stations 312 and 204). This effect is particularly obvious on T4, a transect which was almost completely covered by sea ice at the time of sampling. In contrast, highest concentrations were observed east of the ice edge, on transects T5 ($[BSi]_{max}$ = 1.89 µmol L^{-1} at st. 512, $[BSi]_{max}$ = 2.15 µmol L^{-1} at st. 507), T2 ($[BSi]_{max}$ = 1.70 µmol L^{-1} at st. 207) and T3 ($[BSi]_{max}$ = 2.01 µmol L^{-1} at st. 309). On T5, BSi was accumulated mainly in the upper 30 m, whereas on T3, the peak of BSi was first located within the upper 30 m (stations 312 and 309), then extended downward to depths of 90–180 m at the easternmost st. 300, with moderate concentrations (0.47–0.57 µmol L^{-1}).

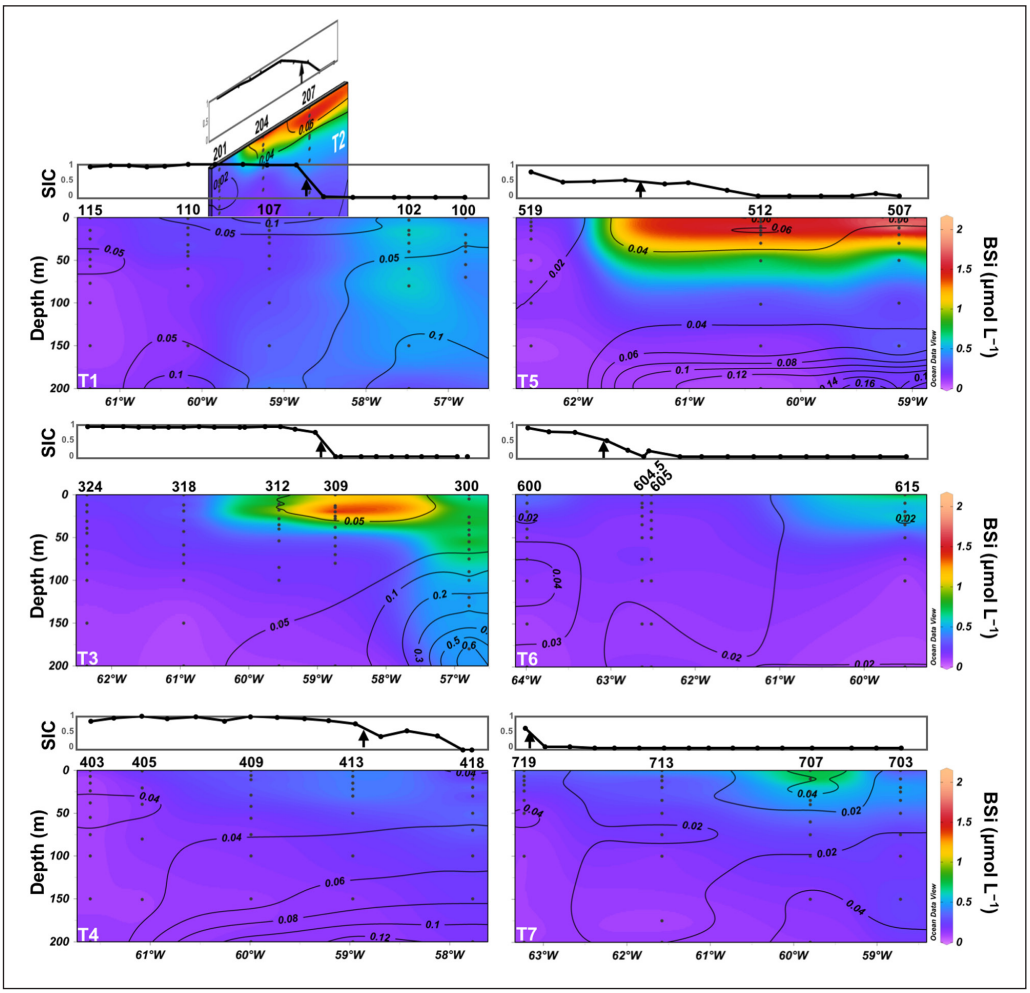

Figure 5: Vertical distribution of biogenic silica concentrations along the seven transects. Biogenic silica (BSi) is expressed in µmol L^{-1}. Contour lines represent lithogenic silica (LSi), expressed in µmol L^{-1}. Sea ice concentrations (SIC) are shown in the graph above each transect. The black arrow in those graphs indicates the location of the ice edge (SIC = 0.5). DOI: https://doi.org/10.1525/elementa.382.f5

The BSi accumulation area observed at stations 309, 204 and 207 decreased in intensity southward but was still visible in the eastern part of T1 (st. 102), also characterized by moderate BSi concentrations (0.47–0.61 µmol L^{-1}) to 150-m depth. BSi distribution along T6 and T7 followed a different pattern, with low concentrations (<0.53 µmol L^{-1}), except in very specific areas (stations 615 and 707) located far from the ice edge, where moderate concentrations (up to 0.89 µmol L^{-1}) were measured.

The vertical distribution of LSi (**Figure 5**) indicated low concentrations (<0.15 µmol L^{-1}) at every station, except at st. 300 where LSi reached 0.74 µmol L^{-1} at 180-m depth, which is probably a result of proximity to the seabed. This station was located on the Greenland shelf, and characterized by a relatively shallow bottom depth of 196 m. Ragueneau and Tréguer (1994) showed that a fairly constant percentage of siliceous lithogenic material (up to 15% for a coastal environment) can dissolve during the first alkaline digestion, resulting in an overestimation of BSi when water samples are enriched with LSi. However, using this upper 15% value, we estimate that the LSi interference was less than 0.025 µmol L^{-1} for most of our samples. Corresponding BSi concentrations were always much higher, even at st. 300 where LSi contamination could have reached 0.11 µmol L^{-1}. In addition, plotting LSi versus BSi did not yield a significant linear relationship ($r = 0.04$; $p = 0.44$), suggesting that LSi concentrations were too low to significantly bias our BSi measurements.

Biogenic silica uptake rates

Si uptake rates (ρSi) (**Figure 6**) generally followed the BSi distribution, with lower ρSi at the westernmost ice-covered stations and highest values centred around the two BSi accumulation areas located on T2, T3, and T5. The highest ρSi was located at st. 309 at 20-m depth (0.19 µmol L^{-1} d^{-1}). Si uptake rates were also high at stations 312 (up to 0.10 µmol L^{-1} d^{-1}) and 204 (up to 0.12 µmol L^{-1} d^{-1}), which were covered by sea ice but located close to the ice edge. On transect T5, the highest Si uptake rate (0.10 µmol L^{-1} d^{-1}) at st. 507 matched the peak of BSi (2.15 µmol L^{-1}) located at 12-m depth, whereas at st. 512, the peak of Si uptake was located below the peak of BSi (ρSi_{max} = 0.12 µmol L^{-1} d^{-1} at 30 m; BSi_{max} = 1.89 µmol L^{-1} at 15 m). Si uptake was low throughout transects T4 and T1 (<0.02 µmol L^{-1} d^{-1}) except below the sea ice at stations 107 and 409 where ρSi was moderate (0.05–0.06 µmol L^{-1} d^{-1}). Along T6, a local peak of production (0.10 µmol L^{-1} d^{-1}) was measured at st. 615 at 25-m depth, matching both the

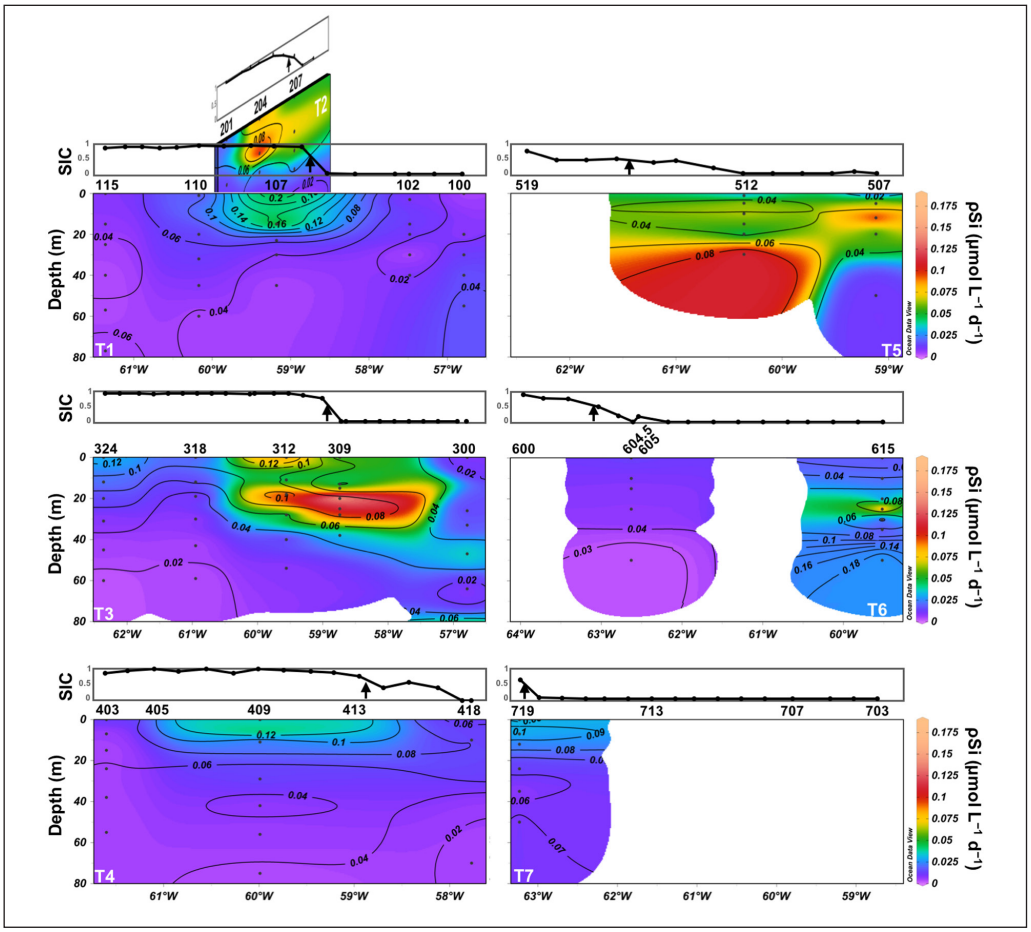

Figure 6: Vertical distribution of Si uptake rates along the 7 transects. Si uptake rate (ρSi, in µmol L^{-1} d^{-1}) was measured from the surface to the depth at which 0.1% of the surface PAR remained. Contour lines represent the specific Si uptake rate (VSi, in day^{-1}). Sea ice concentrations (SIC) are shown in the graphs above each transect. The black arrow in those graphs indicates the location of the ice edge (SIC = 0.5). For T5–T7, ρSi and VSi were not interpolated throughout the transect because of lack of data. DOI: https://doi.org/10.1525/elementa.382.f6

SCM and BSi maximum measured at this station. Station 719, which was located close to the ice edge of T7 was characterized by very low ρSi values (<0.03 μmol L^{-1} d^{-1}).

Specific Si uptake rates (VSi) (**Figure 6**) were clearly higher below the sea ice at stations close to the ice edge (0.11–0.16 d^{-1} at stations 204, 312, 409, and 719), with a maximum observed at st. 107 (0.23 d^{-1}). Stations 204 and 312 were associated with high BSi concentrations, indicating that the biomass had had time to accumulate, whereas BSi was still low at stations 107, 409, and 719, which could be indicative of an early bloom stage. On T5, VSi was low at the easternmost st. 507 (<0.05 d^{-1}), whereas a subsurface maximum was measured at st. 512 (0.10 d^{-1} at 30 m), matching the ρSi peak. On T6, VSi was low at st. 604.5 (<0.05 d^{-1}), but two subsurface VSi peaks were measured at st. 615 (0.12 d^{-1} at 25 m; 0.20 d^{-1} at 50 m).

Diatom assemblage structure

Absolute abundance and carbon biomass

In total, 47 diatom taxa were identified to the species or genus level in this study. The taxa are listed in Table S4.

Diatom abundance (**Figure 7a, b**) was highly variable throughout the study area, ranging in surface waters from 1,000 cells L^{-1} at st. 418 to 916,000 cells L^{-1} at st. 204, the latter being covered by sea ice (SIC = 0.93) but located close to the ice edge. As a general tendency, higher abundances were found at ice-free stations (185,000 to 624,000 cells L^{-1}, at stations 309, 507, 512, and 707), and closely matched the two BSi accumulation areas (**Figures 4c** and **5**). Abundances were low to moderate (<79,000 cells L^{-1}) for the other stations, independently of ice cover. The depth of the TChl *a* maximum varied among stations, and was located between the surface and 44 m. At the SCM, diatom abundances followed a pattern of distribution similar to that observed at the surface, with higher abundances observed on transect T5 (484,000 and 610,000 cells L^{-1} at stations 507 and 512), and close to the ice edge of transects T2 and T3 (119,000 to 464,000 cells L^{-1} at stations 204, 207, and 309), both on the western and eastern sides of this limit.

Total diatom carbon biomass (**Figure 7c, d**) for surface and SCM varied, respectively, from 0.1 (st. 418) to 149.0 μg C L^{-1} (st. 507) and from 0.1 (st. 418) to 210.0 μg C L^{-1} (st. 507). Throughout the study area, most of the stations exhibited low to very low carbon biomass (<20.0 μg C L^{-1}), with the exception of stations 204, 207, 309, 507, and 512, both at the surface (75.1 ± 49.3 μg C L^{-1}, n = 5) and at the SCM (116.1 ± 64.2 μg C L^{-1}, n = 5). Station 707 was characterized by an intermediate diatom carbon biomass (25.3 μg C L^{-1}), but only at the surface.

Relative abundance and carbon biomass

Regarding cell numbers, the five taxa that dominated the diatom assemblages were (**Figure 8a, b**): *Chaetoceros* spp. (mean ± sdv for the 43 samples counted: 19 ± 26%; mostly *C. gelidus* and *C. decipiens*), *Pseudo-nitzschia* spp. (17 ± 23%), *Ceratoneis closterium* (14 ± 16%), *Fragilariopsis* spp./*Fossula arctica* (13 ± 16%), and *Thalassiosira* spp. (9 ± 9%; mostly *T. antarctica var. borealis, T. gravida*, and *T. nordenskioeldii*). *Fragilariopsis* spp. and *Fossula arctica* were grouped together because of the difficulty in distinguishing the two taxa with light microscopy in some samples.

At the surface, a distinct diatom assemblage was located within the main BSi accumulation areas (stations 204, 207, 300, 309, 507, 512, 703, and 707; **Figure 4c**). These stations (n = 8) were characterized by a larger contribution of *Chaetoceros* spp. (56 ± 18%) and also by a moderate proportion of *Thalassiosira* spp. (12 ± 7%). In contrast, at the other surface stations (n = 15), the diatom assemblage was dominated by *Ceratoneis closterium* (26 ± 19%) and by

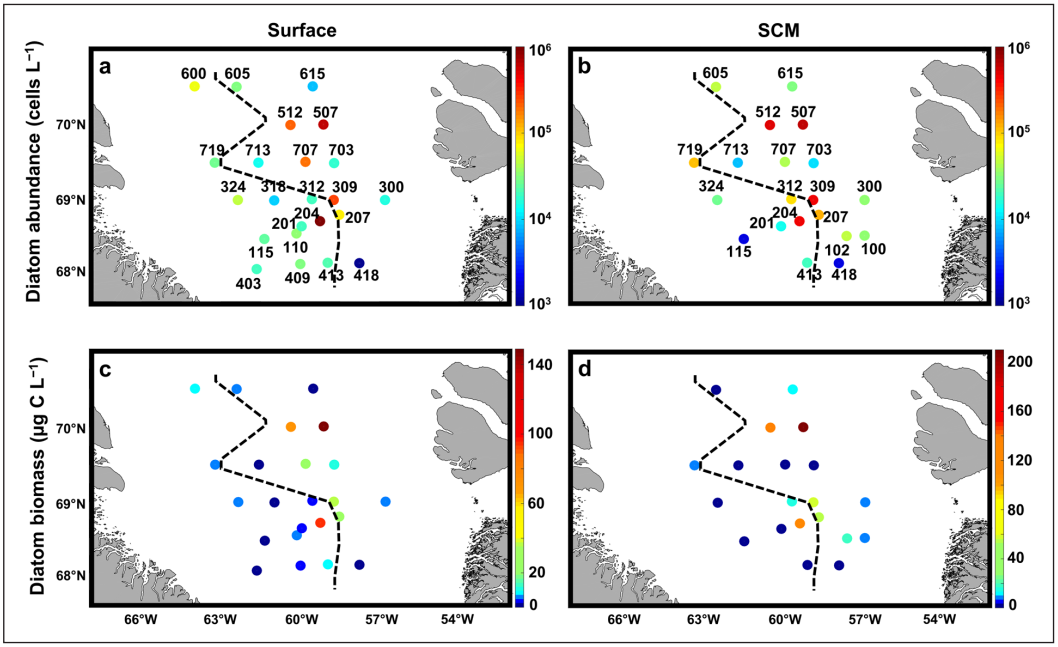

Figure 7: Absolute diatom abundance and carbon biomass. Live diatom cell abundance (cell L^{-1}) at the surface **(a)** and the subsurface chlorophyll *a* maximum (SCM) **(b)**. Live diatom carbon biomass (μg C L^{-1}) at the surface **(c)** and the SCM **(d)**. The black dashed lines correspond to the approximate location of the ice edge at the time of sampling.
DOI: https://doi.org/10.1525/elementa.382.f7

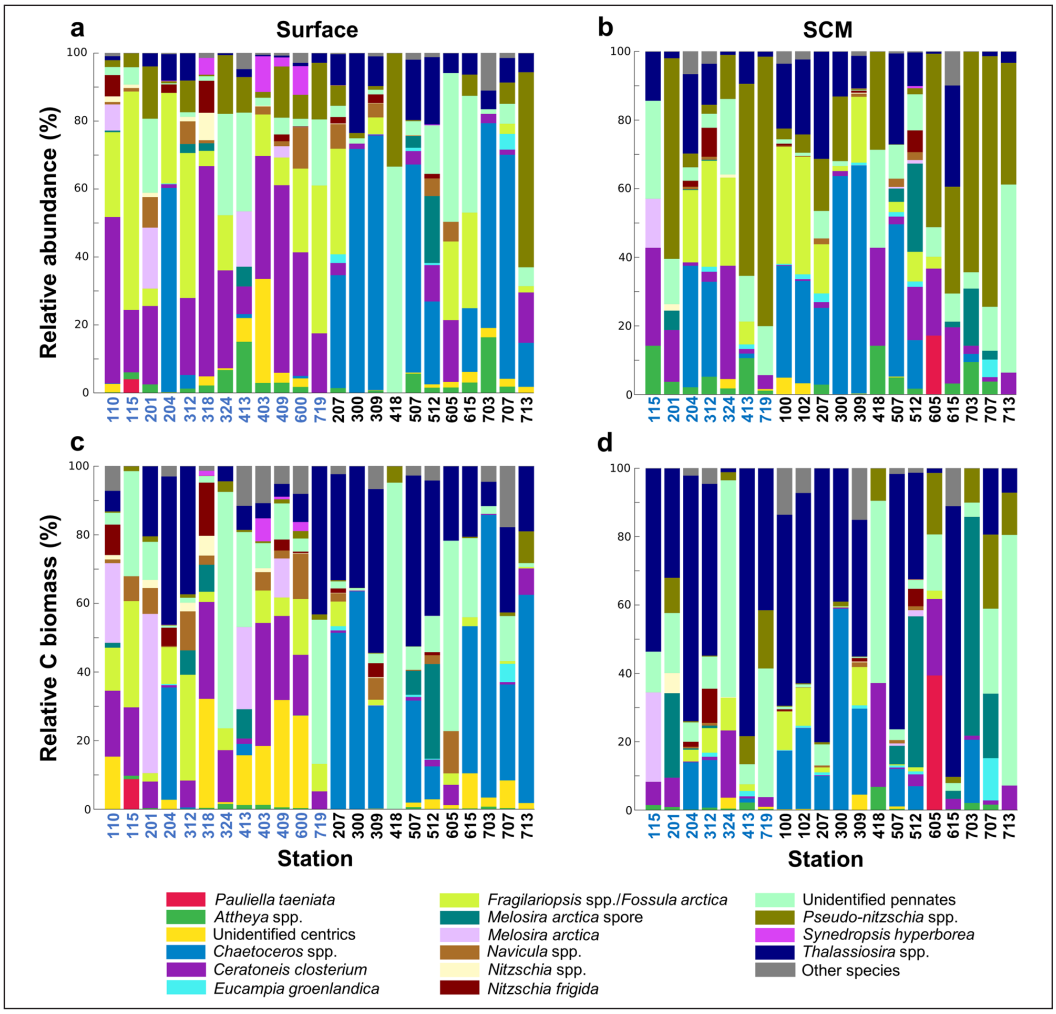

Figure 8: Relative diatom abundance and carbon biomass. Relative abundance (%) of each diatom taxon at the surface **(a)** and the subsurface chlorophyll *a* maximum (SCM) **(b)**. Relative carbon biomass (%) of each taxon at the surface **(c)** and the SCM **(d)**. The station numbers for ice-covered locations (SIC > 0.5) are indicated in blue font on the bottom axis. DOI: https://doi.org/10.1525/elementa.382.f8

Fragilariopsis spp./*Fossula arctica* (20 ± 19%). The following ice-associated species were also observed at the surface: *Melosira arctica* vegetative cells (13 ± 10% at stations 110, 201, 413, and 409), *Synedropsis antarctica* (7 ± 3% at stations 318, 403, 409, and 600), and *Nitzschia frigida* (4 ± 3% at stations 110, 204, 318, 409, 207, 309, and 512).

At the SCM, two distinct diatom assemblages were also observed. Similarly to the surface, one assemblage was located where a diatom bloom was taking place (stations 204, 207, 309, 312, 507, and 512) or probably had occurred (stations 100, 102, and 300), according to BSi and ρSi data (**Figures 5** and **6**). This assemblage (n = 9) was also characterized by a larger proportion of *Chaetoceros* spp. (37 ± 18%) and variable proportions of *Fragilariopsis* spp./*Fossula arctica* (19 ± 13%) and *Thalassiosira* spp. (18 ± 8%). Excluding stations 115 and 418 where diatom abundances were extremely low, the other SCM stations (n = 9) were largely dominated by *Pseudo-nitzschia* spp. (56 ± 17%) and by some unidentified pennate diatoms (16 ± 16%).

On two occasions, *Melosira arctica* resting spores contributed importantly to relative abundance: at stations 512 (surface: 20%; SCM: 26%) and 703 (SCM: 17%). Although we had not expected to observe such a high contribution of an ice-associated diatom at st. 703 (DOW50 = 23 days), it represents only 1.8×10^3 spores L^{-1} in terms of absolute abundances, as diatom abundances at this station were very low. *Melosira* spp. resting spores were also observed with a contribution <6% at stations 312, 318, 413, 207, and 507. Resting spores of *Thalassiosira antarctica var. borealis* (data not shown) were rare but were identified at stations 100, 102, and 615 (up to 3.0×10^3 spores L^{-1}).

When converted to carbon biomass (**Figure 8c, d**), the contribution of centric diatoms increased at all stations, even at some stations where pennate diatoms largely dominated in terms of abundances. This increase is particularly obvious for *Thalassiosira* spp., which accounted for 21 ± 17% of diatom C biomass at the surface taking into account all of the stations (n = 23), and 41 ± 29% at the SCM (n = 20), but also for *Melosira arctica* vegetative cells (26 ± 15% at the surface of stations 110, 201, 409 and 413). *Chaetoceros* spp. C biomass accounted for 19 ± 26% at the surface (n = 23) and 10 ± 14% at the SCM (n = 20), and was largely associated with the main diatom accumulation areas. Conversely, pennate diatoms such as *Ceratoneis closterium* and *Fragilariopsis* spp./*Fossula arctica*, which were key contributors to one of the two assemblages observed at the surface, accounted for a much lower

biomass at those same stations (respectively, 13 ± 11% and 7 ± 8%, n = 15), due to their lower biovolumes. This trend was also true for *Pseudo-nitzschia* spp., a taxon that was observed to dominate one of the two assemblages at the SCM, and had a low contribution to C biomass at those same stations (11 ± 7%, n = 9). The category 'Other species' which is composed of rare (i.e., *Rhizosolenia* spp., *Coscinodiscus* spp., *Porosira glacialis, Entomoneis* spp., *Bacterosira bathyomphala*, etc.) and mostly large taxa, was important in terms of diatom C biomass at some stations, with up to 18% in the surface at st. 707.

Taxon-specific contributions to silica production

The contribution of each taxon to biogenic silica production was investigated using PDMPO epifluorescence image analysis (see Figure S7 for illustrations) for the five most productive stations (i.e., with the highest ρSi) in order to identify the most actively silicifying species at locations where a diatom bloom was taking place. For those stations, relative abundance, biomass and species-specific silicification contributions have been presented together for comparison (**Figure 9**). *Thalassiosira* spp. (mostly *T. antarctica var. borealis and T. gravida*) strongly dominated BSi production at the SCM at stations 309 and 507 (respectively, 85 and 93%). At these stations, *Thalassiosira* spp. contributions increased successively between abundance (respectively, 9 and 27%), C biomass (respectively, 40 and 75%), and Si production. Conversely, *Chaetoceros* spp. (mostly *C. gelidus*) were major contributors to cell abundance (up to 60%), but were negligible in terms of BSi production, due to their small biovolume and weak degree of silicification. The fluorescence of *C. gelidus* was often low and difficult to detect, such that some labelled *C. gelidus* cells may have been missed, but an under-estimation would not have affected our results significantly, as fluorescence per *C. gelidus* cell was much lower than the fluoresence of the other taxa. *Melosira arctica* resting spores were actively silicifying at the SCM at st. 512, contributing 82% of Si production, while they contributed only 26% of abundance and 44% of C biomass. *Chaetoceros* spp., mostly *C. decipiens*, were very active in the surface at st. 207 (32%) and also important contributors to both abundance (33%) and biomass (51%). Two very rare taxa contributed significantly to Si production in two surface locations: *Coscinodiscus* spp. (19%) at st. 204 and *Rhizosolenia* spp. (38%) at st. 207. Due to a large surface area, *Coscinodiscus* spp. were characterized by the highest silicifying activity per cell (i.e., PDMPO fluorescence). *Fragilariopsis* spp./*Fossula arctica* were actively silicifying mainly in the surface at ice-covered st. 204 (21%), while they were also important contributors to abundance in the surface at st. 207 and at the SCM at St. 309. The sea ice diatom *Nitzschia frigida* was only found active in the surface at the ice-covered station 204 (16%).

Discussion

During the Green Edge expedition, the development of the late spring–early summer diatom bloom was studied in relation with the sea ice retreat. Through this study, we have attempted to fully describe the diatom bloom dynamics in central Baffin Bay, by describing diatom assemblage structures and carbon biomass, and silica uptake activities at both the assemblage and the genus/species level. A cluster analysis, performed to summarize the main results (**Figures 10** and **11**, **Table 1**), is discussed in the following sections.

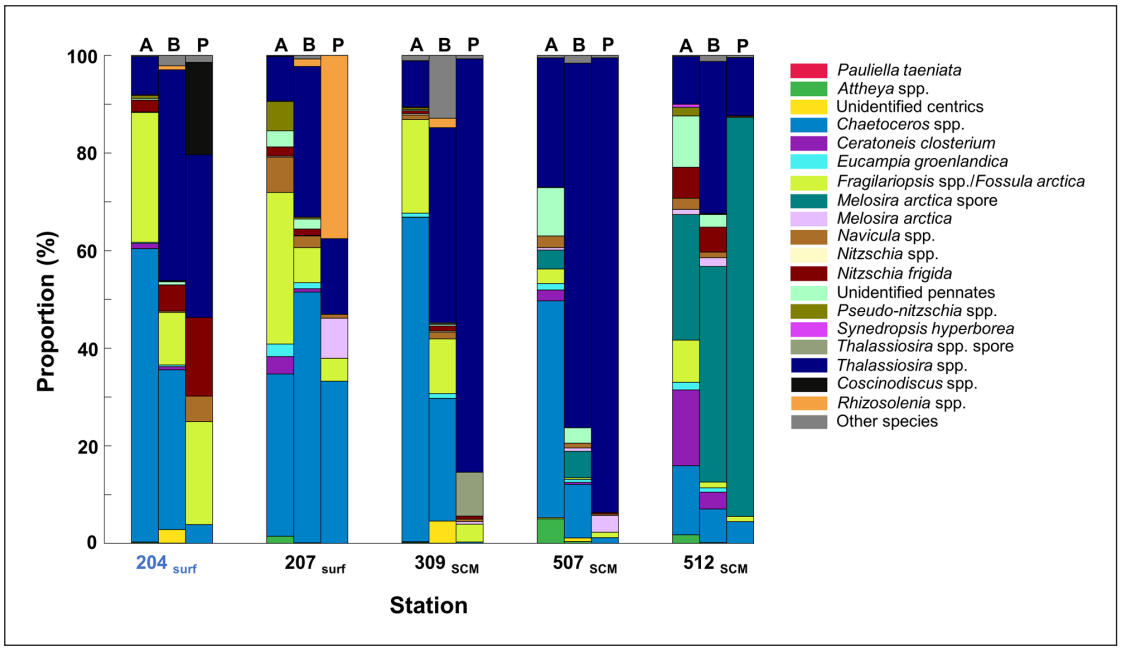

Figure 9: Taxon-specific contribution to biogenic silica deposition at the five most productive stations. For each station, relative abundance (A), carbon biomass (B) and PDMPO fluorescence (P) are presented for comparison. Station 204 was covered by the ice pack (SIC > 0.5). The taxa *Coscinodiscus* spp., and *Rhizosolenia* spp., as well as spores of *Thalassiosira* spp. were extracted from the category 'Other species' in order to show their importance in terms of contribution to BSi deposition. DOI: https://doi.org/10.1525/elementa.382.f9

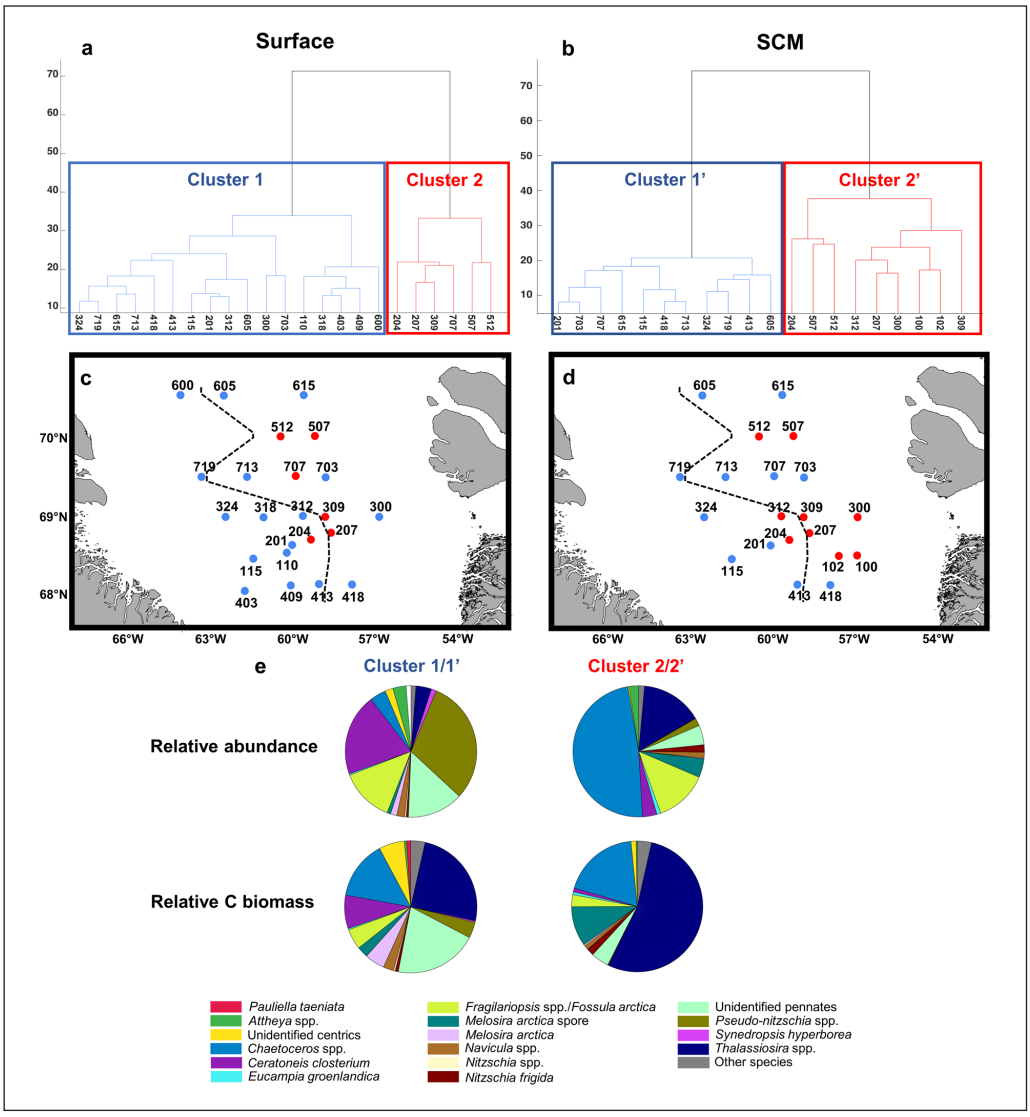

Figure 10: Cluster analysis performed on abundance data from surface and subsurface chlorophyll *a* maximum samples. The dendrogram displays the similarity relationship among samples in terms of their taxonomic composition, for the surface **(a)** and the subsurface chlorophyll *a* maximum (SCM) **(b)**. Map of the study area with the stations colored according to the cluster they belong to (blue for clusters 1 and 1′; red for clusters 2 and 2′), for the surface **(c)**, and the SCM **(d)**. The black dashed lines correspond to the approximate location of the ice edge at the time of sampling. **(e)** Relative abundance and relative carbon biomass for the 'mean' assemblages associated with the two clusters. Clusters 1 and 2 were not statistically different from, respectively, clusters 1′ and 2′ and were therefore grouped together, giving clusters 1/1′ and 2/2′. DOI: https://doi.org/10.1525/elementa.382.f10

Characterization of the diatom bloom: Development in relation with the hydrographic conditions

The cluster analysis (**Figure 10a, b**) performed separately on surface and SCM abundance data identified four clusters of stations. ANOSIM one-way analysis compared each pair of clusters and showed that clusters 1 and 2 were not statistically different from clusters 1′ and 2′, respectively (p-values from pairwise analyses were equal, respectively, to 0.08 and 0.38). Hence, hereafter we will only distinguish the two statistically different clusters 1/1′ and 2/2′, which were observed both at the surface and the SCM.

The cluster 2/2′ stations were associated with the highest integrated Chl *a* and BSi measured in Baffin Bay (81.5 ± 29.0 mg m^{-2} and 56.1 ± 18.5 mmol m^{-2}, respectively) (**Table 1**). Integrated Si uptake rates indicate that this diatom assemblage was actively silicifying (1.70 ± 0.93 mmol m^{-2} d^{-1}), except at the easternmost stations 100, 102, and 300, where ρSi was low and BSi was moderate down to 180-m depth, suggesting a post-bloom stage with diatoms that were probably settling out of the upper mixed layer. Cluster 2/2′ was associated on average with a much higher contribution to total particulate organic carbon (POC) than cluster 1/1′ (**Table 1**). Cluster 2/2′ represented on average 22% of POC, while cluster 1/1′ only represented 3% of POC. The record contribution of diatoms to C biomass was reached at st. 507, contributing as much as 41% of POC at the surface and 66% at the SCM. Hence, depending on the station, diatoms of cluster 2/2′ were either actively blooming or corresponded to a remnant bloom that had occurred a few days or a few weeks before sampling. The cluster 2/2′ stations were mainly located east of the ice edge on transects T1–T3 and

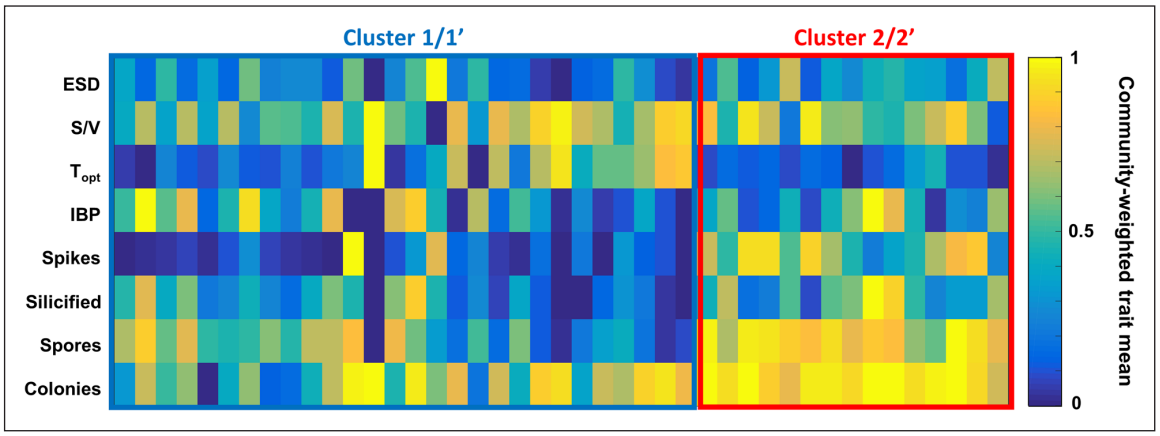

Figure 11: Community-weighted trait means of diatom species found in cluster 1/1′ and 2/2′. The color bar indicates the value of the normalized community-weighted trait means (0 to 1) for clusters 1/1′ (framed in blue) and 2/2′ (framed in red). The eight traits include equivalent spherical diameter (ESD), surface area to volume ratio (S/V), optimum temperature for growth (T_{opt}), ability to produce ice-binding proteins (IBP), presence or absence of long, sharp projections such as setae, spines, horns and cellular processes ('spikes'), degree of silicification ('silicified') qualitatively based on examination of SEM images, propensity to form resting spores ('spores'), and ability to form colonies ('colonies'). Each trait was normalized in relation to the stations that presented the lowest (= 0) and the highest values (=1). DOI: https://doi.org/10.1525/elementa.382.f11

Table 1: Mean and standard error of hydrographic and biological parameters for each cluster. DOI: https://doi.org/10.1525/elementa.382.t1

Parameters[a]	Cluster 1/1′	Cluster 2/2′
DOW50 (d)	−5 ± 15	5 ± 9
SIC	0.61 ± 0.44	0.19 ± 0.36
hBD (m)	20 ± 4	21 ± 10
Ze (m)	32 ± 9	27 ± 8
ANP_20 m (%)	27 ± 18	7 ± 4
$[NO_3^-]$ (μM)	3.47 ± 2.40	1.33 ± 2.09
$[H_4SiO_4]$ (μM)	5.43 ± 3.05	1.63 ± 1.34
$[PO_4^{3-}]$ (μM)	0.56 ± 0.25	0.24 ± 0.17
$[H_4SiO_4]$: $[NO_3^-]$	5.06 ± 9.23	7.37 ± 10.15
Temperature (°C)	−1.02 ± 1.04	−0.88 ± 0.75
Salinity	32.70 ± 0.70	32.83 ± 0.64
∫ Chl *a*_80 m (mg m^{-2})	40.03 ± 36.16	81.52 ± 28.96
∫ BSi_80 m (mmol m^{-2})	19.03 ± 6.78	56.07 ± 18.53
∫ ρSi_0.1% PAR (mmol m^{-2} d^{-1})	0.73 ± 0.31	1.70 ± 0.93
∫ VSi_0.1% PAR (d^{-1})	3.37 ± 0.66	1.58 ± 0.53
Live cell abundance (cells L^{-1})	33.9 × 10^3 ± 25.9 × 10^3	305.9 × 10^3 ± 267.9 × 10^3
C biomass (μg C L^{-1})	3.87 ± 3.13	68.88 ± 60.93
Diatom contribution to POC (%)	3 ± 2	22 ± 17

[a] For parameters characterizing the whole station (DOW50, SIC, hBD, Ze, ANP at 20 m, and integrated parameters), only the stations that belonged to the same cluster both at the surface and the SCM were included in the calculation of the mean and standard deviation (n = 15 and 7 for clusters 1/1′ and 2/2′, respectively). For parameters that can take different values at the surface and the SCM (nutrient concentrations, temperature, salinity, live cell abundance, C biomass and diatom contribution to POC), we used all the stations and depths for the calculations (n = 28 and 15 for clusters 1/1′ and 2/2′, respectively). Chl *a* and BSi were integrated to a depth of 80 m, while ρSi and VSi were integrated to the depth at which 0.1 % of the surface PAR remained (Ze). Please see text for definition of abbreviations.

T5 (**Figure 10c, d**), in waters where the sea ice was at an advanced state of melting (SIC = 0.19 ± 0.36; DOW50 = 5 ± 9 days) and with shallower euphotic zone depths (Ze) (**Table 1**). This observation is in accordance with the classical picture of an Arctic ice-edge phytoplankton bloom starting as a band along the ice edge and developing in

the wake of the melting ice (Sakshaug and Skjoldal, 1989; Perrette et al., 2011). The melting of the ice pack causes both an increase in the amount of solar irradiance at the surface and the formation of a shallow and low density layer, which is usually nutrient-replete after the winter season (Smith and Nelson, 1985; Sakshaug and Skjoldal, 1989), i.e., fulfilling all the conditions known to be critical for the onset of a bloom (Chiswell et al., 2015). Cluster 2/2′ stations were also found in low-% ANP waters compared to cluster 1/1′ (**Table 1**), indicating a preferential development in Atlantic-influenced waters at this stage. The development of cluster 2/2′ diatoms to elevated abundances and biomasses resulted in a strong depletion of all nutrients, which were consumed down to detection levels at the surface of several stations, and did not exceed 0.6 μmol L^{-1} for NO_3^-, 1.4 μmol L^{-1} for H_4SiO_4, or 0.2 μmol L^{-1} for PO_4^{3-}.

However, another scenario was also observed along the northern transects T6 and T7, where the diatom development at the ice edge was weaker. The ice-free stations 605 and 713, located in the vicinity of the ice edge, belonged to cluster 1/1′ (**Figure 10**), which was characterized by lower Chl *a* (40.0 ± 36.2 mg m^{-2}), lower BSi concentrations (19.0 ± 6.8 mmol m^{-2}), and lower silica uptake activities (0.7 ± 0.3 mmol m^{-2} d^{-1}) (**Table 1**). At those two stations, nutrients were not completely exhausted by biological activity in comparison to the stations located in proximity to the ice edge on the southern transects T1–T4. The last two transects, T6 and T7, were sampled later during the melting season, enabling the icebreaker to reach ice-free waters highly influenced by Pacific waters, according to the ANP index which was equal to 40% at st. 604.5. This water mass originates from the Bering Sea and is known to enter Baffin Bay from the northern Lancaster, Jones and Smith sounds before mixing with Baffin Bay waters (Tremblay, 2002; Tang et al., 2004). The resulting Pacific-influenced waters are enriched in phosphate and orthosilicic acid relative to nitrate, and also exhibit very different T-S signatures compared to Baffin Bay waters (Figure S2). Randelhoff et al. (2019) estimated the depth of the last winter overturning, and showed it was deeper at the eastern Atlantic-influenced stations (50 m vs 34 m at the Pacific-influenced stations), where it reached the underlying nutrient reservoir. This nutrient-rich layer is shallower in the east, and thus easier to reach. Therefore, the estimated pre-bloom nitrate inventory was higher in the east vs. west (11 vs 5–6 μmol L^{-1}), which may have modulated the maximum accumulation biomass and kinetic parameters such as the maximum growth rate. Perrette et al. (2011; **Figure 4** therein) also pointed out that, in Baffin Bay, the bloom tends to weaken as it moves westwards. Surface Chl *a* images derived from satellite over the April–August 2016 period (Figure S8) show a similar pattern of development for the sampling period, indicating that this scenario may be common.

Most of the western stations located under the ice pack belonged to the low productive cluster 1/1′. Nevertheless, high VSi values (**Table 1**) were observed associated with this cluster, especially below the ice pack in the vicinity of the ice edge (stations 107, 409, and 719), indicating that the cluster 1/1′ diatom assemblage was probably growing at these stations and may have initiated the onset of the diatom bloom, although it did not have sufficient time to accumulate and/or was already subject to zooplankton grazing. Some of the easternmost stations (418, 703, and 300 at the surface) also belonged to cluster 1/1′, which can be attributed to very low diatom abundances at these locations due to post-bloom conditions. Because the cluster analysis was performed on absolute abundances rather than relative abundances, stations with very low abundances tend to cluster together. This effect is particularly obvious for st. 300 at the surface, where the diatom assemblage structure was similar to that observed for cluster 2/2′ (see next section for details), but belonged to cluster 1/1′ due to very low cell abundances.

On certain occasions (at stations 204 and 312), the diatom bloom could extend beneath the pack ice (SIC = 0.93 to 1.00), 20 to 30 km away from the ice edge. Using typical open-ocean horizontal diffusivities, Randelhoff et al. (2019) concluded that this biomass was unlikely to have been advected from less ice-covered stations. Our Si uptake rate measurements tend to support their results by showing that the diatom biomass observed under the pack ice was actively silicifying. Massive blooms of diatoms have already been reported under the ice, extending sometimes more than 100 km into the ice pack (Arrigo et al., 2012; Laney & Sosik, 2014; Mundy et al., 2014), suggesting that sea ice cover is not the only factor controlling the amount of light transmitted through the ice. This amount also depends on the depth of the snowpack covering the ice (Mundy et al., 2005), the formation of melt ponds (Arrigo et al., 2014), the presence of leads in the ice pack (Assmy et al., 2017), and the presence or absence of an ice algal bloom at the bottom of the sea ice (Mundy et al., 2007). In their study, Randelhoff et al. (2019) examined the light transmittance in the upper 100 m of the water column, both at the open water and ice-covered stations sampled during the Green Edge expedition. They pointed out that light transmittance under the ice pack was lower than 0.3, whereas at the open water stations it was higher than 0.8 at the surface. However, transmittance under the ice was strong enough that even at ice concentrations close to 1, the depth of the euphotic zone (Ze) was located between 15 and 30 m, and was almost always located below the depth of the equivalent mixed layer. These findings imply that phytoplankton growth was not disrupted by mixing out of the euphotic zone. They concluded that light transmittance was sufficient to allow net phytoplankton growth far into the ice pack (where SIC is close to 1). Although the bloom initiation probably began under the compact ice pack, it took time for the biomass to accumulate, which may explain why the peak of biomass was observed later in the melting season (Randelhoff et al., 2019).

Considering that cluster 2/2′ stations were representative of the diatom bloom, the bloom lifetime can be estimated, according to DOW50 data, to last between 18 and 27 days locally. Stations 204 and 309, located in the core of the actively silicifying diatom bloom, were characterized by a DOW50 equal to −12 and 6 days, respectively (total: 12 + 6 = 18 days of bloom), whereas at st. 102, diatoms were not silicifying anymore and DOW50 was

equal to 15 days (total: 12 + 15 = 27 days). These lifetime estimates are in full agreement with Perrette et al. (2011) who demonstrated, using satellite ocean colour data, that half of the ice-edge blooms in the Arctic ended within 20 days. The absence of a diatom bloom at the easternmost stations of T4 (st. 418) and T7 (st. 703), which belonged to cluster 1/1′, can thus be explained by the DOW50 (23 days at both stations), implying that a bloom could have begun at least 35 days before sampling, as a bloom has been found to occur as early as 12 days before SIC = 0.5. In addition, high phaeophorbide *a* concentrations were measured at st. 418, which may be evidence for intensive top-down control by grazers at this station. According to the Si:N:P molar ratios, diatom development in the ice-free Atlantic-influenced waters could be limited potentially first by nitrate in the upper 20–30 m of the water column corresponding to the euphotic layer (Ze = 27 ± 8 m), which would have caused the termination of the diatom bloom at the easternmost stations (100, 102, and 300). In response to this nutrient limitation in surface waters, Randelhoff et al. (2019) observed the Chl *a* maximum to deepen towards the east (Figure S3), staying below the nitracline and above the depth of the euphotic zone, where the compromise between availability of nutrients and light availability was optimal. Overall, these observations are in good agreement with the study of Tremblay and Gagnon (2009), who proposed that the onset of the bloom is controlled primarily by the amount of light, but that the magnitude of the annual primary production in seasonally ice-free waters is controlled mainly by the nitrogen supply.

Inside the diatom bloom: assemblage structure, biomass and taxon-specific contribution to BSi production

As detailed above, two statistically different diatom assemblages were identified from the cluster analysis (**Figure 10**): overall, the cluster 2/2′ was associated with the core of the diatom bloom, whereas cluster 1/1′ was much less productive. The cluster 1/1′ assemblage (**Figure 10e**) was composed primarily of *Pseudo-nitzschia* spp. (mostly *P. delicatissima*), *Ceratoneis closterium*, ribbon-forming species belonging to *Fragilariopsis* spp. (mostly *F. cylindrus* and *F. oceanica*), *Fossula arctica*, and some unidentified pennate diatoms. In contrast, the cluster 2/2′ assemblage was dominated by centric diatoms, primarily *Chaetoceros* spp. (mostly *C. gelidus*) and *Thalassiosira* spp. (mostly *T. antarctica var. borealis and T. gravida*), and to a lesser extent, pennate diatoms belonging to *Fragilariopsis* spp. and *Fossula arctica*. Aside from *P. delicatissima*, these species are commonly reported as the most important diatom species quantitatively during spring blooms in the Arctic (Quillfeldt, 2000; Quillfeldt, 2001; Booth et al., 2002; Poulin et al., 2011). Assemblages 1/1′ and 2/2′ fit into the classic successional pattern described for Arctic spring blooms: ribbon-forming pennate species blooming before centric diatoms belonging to *Chaetoceros* spp. and *Thalassiosira* spp, with *Fragilariopsis* spp. sometimes remaining for longer periods, even co-occurring with the centric diatom bloom (Quillfeldt, 2000; Booth et al., 2002; Hodal et al., 2012). The *Thalassiosira* spp. bloom is often described as being intense and transient, and rapidly replaced by a *Chaetoceros* spp. bloom, usually dominated by *C. gelidus*, which is able to maintain its population at low nutrient levels (Booth et al., 2002). However, in our study, *Thalassiosira* spp. and *Chaetoceros* spp. were always observed as co-occurring groups.

Excluding st. 512 where we observed high abundances of the sea ice diatom *Melosira arctica*, the observed pelagic diatom bloom is unlikely to have been associated with the release of sea ice diatoms from the ice pack. Indeed, most of the species encountered in cluster 2/2′ are known to be pelagic, apart from some *Fragilariopsis* species and *Fossula arctica* which, though often observed in ice cores (Quillfeldt, 2000), represented only 13% of the assemblage. Furthermore, according to ice samples that were collected in May–June of the same year at an ice camp located close to our sampling area (Massicotte et al., 2019), ice-diatom assemblages were dominated mainly by the species *Nitzschia frigida* (65% of the diatoms, n = 6 samples). In our samples, this species was very rare, which tends to support the view that ice diatoms were not important contributors to the pelagic bloom.

In this study, the chlorophyll c_3 pigment was also used as a proxy for *Phaeocystis* spp. biomass (Stuart et al., 2000; Antajan et al., 2004). High integrated Chl c_3 concentrations were observed at stations 512 and 615, where in addition the Chl c_3:TChl *a* ratio was close to 0.20, which is typical of *Phaeocystis* species (Stuart et al., 2000; Antajan et al., 2004). Data from prymnesiophyte counts confirm that *Phaeocystis* spp. largely dominated the protist community at these two stations (up to 11.0×10^6 cells L^{-1}), but also at stations 204 and 207 (see Figure S6 for data on *Phaeocystis* spp. abundances). The intense subsurface peak of Chl *a* at st. 615 (12.8 μg L^{-1} at 25m), which corresponds to the maximum recorded throughout the bay, is thus mainly associated with *Phaeocystis* spp., as diatom biomass at this station was low (<10.3 μg C L^{-1}) and only represented 2–3% of the POC. In contrast, *Phaeocystis* spp. and diatoms appeared to bloom together at stations 204, 207 and 512. These results indicate that *Phaeocystis* spp. occurred during all stages of the bloom, from its early development under the melting sea ice (e.g., stations 204 and 207) to its middle and late development in open waters (e.g., stations 512 and 615), and was able to maintain its population in the SCM at stations where nutrients were depleted in surface waters (e.g., st. 615) well after the end of the diatom bloom. This post-bloom population maintenance can be explained by the ability of *Phaeocystis* spp. to increase NH_4 uptake capacity when nutrients are exhausted (Tungaraza et al., 2003) and to form mucilaginous colonies that are more resistant to grazing (Jakobsen and Tang, 2002), which was probably intensive at this station according to phaeophorbide *a* data. Results are in accordance with Degerlund and Eilertsen (2010) who highlighted the occurrence of *Phaeocystis* spp. at every stage of the spring bloom along the northern Norwegian coast and in the Barents Sea, co-occurring with diatoms or sometimes completely dominating the phytoplankton community. In contrast, Hodal et al. (2012) observed *Phaeocystis* spp. dominating only the post-bloom protist communities. *Phaeocystis* spp. development is also probably tightly linked with the water

masses, as this genus is known to be associated with the inflow of Atlantic water into the Arctic Ocean (Nöthig et al., 2015). The higher temperature of the Atlantic waters is assumed to promote blooms dominated by *Phaeocystis* spp. (Metfies et al., 2016; Nöthig et al., 2015).

Several studies have pointed out that cell abundance data are not sufficient to accurately explain the influence a species may have on biogeochemical cycles (Goldman, 1993; Durkin et al., 2012; Leblanc et al., 2012). When looking at their contribution to carbon biomass (**Figure 10e**), a different picture emerges, with centric diatoms, especially *Thalassiosira* spp., becoming the main contributor for the cluster 2/2′ assemblage, but also for the cluster 1/1′ assemblage which was numerically dominated by pennate diatoms. *Chaetoceros* spp. were the second most important contributors to the C biomass for the cluster 2/2′. Our results are in line with two other reports that found *Chaetoceros* spp. to dominate the total phytoplankton carbon biomass in the northern polynya of Baffin Bay and in the Chukchi Sea (Booth et al., 2002; Laney and Sosik, 2014), followed by *Thalassiosira* spp. and *Fragilariopsis* spp. (the latter only in the Chukchi Sea).

Cell species-specific biogenic silica uptake depends on cell size and morphology (Brzezinski, 1985) but also on the degree of silicification, i.e., the volume-normalized cellular silica content (Baines et al., 2010), itself related to the absolute growth rate (McNair et al., 2018). As these parameters can span many orders of magnitude among taxa, the amount of biogenic silica produced is particularly sensitive to the assemblage structure (Durkin et al., 2012). The use of the fluorescent dye PDMPO allowed quantitative measurement of newly deposited silica in individual diatom cells (McNair et al., 2015), as PDMPO is incorporated in a nearly constant ratio with biogenic silica during synthesis of the opal cell wall (Leblanc and Hutchins, 2005). The major contributors to silica production were thus found to be the larger centric species: *Thalassiosira antarctica var. borealis, T. gravida*, *Melosira arctica* resting spores, and *Chaetoceros decipiens*, even though the contribution of pennate diatoms such as *Fragilariopsis* spp./*Fossula arctica* and *Nitzschia frigida* increased under the pack ice. This contributory role of larger centric species is in agreement with the results of McNair et al. (2018) who demonstrated that the surface area of individual species is the dominant factor accounting for variations in silica production between taxa. Nevertheless, according to the same authors, over the longer time scale relevant to bloom dynamics, the influence of the surface area factor decreases while the growth rate becomes the main controlling factor.

Diatom functional traits associated with assemblages

Functional trait analyses are intended to capture key aspects of organism functionalities in the system (Litchman et al., 2007; Litchman and Klausmeier, 2008) and could be used as a tool to predict the response of biological communities to environmental changes (Mcgill et al., 2006). For each station, **Figure 11** depicts the community-weighted trait mean (CWM), an index used to estimate trait variability at the community level. Overall, when comparing the diatom assemblage structure of the two clusters, the following traits emerge for the species belonging to cluster 2/2′: a higher propensity to produce resting spores and to form colonies, the property to possess extensions such as setae, and cellular processes. The dominant species of cluster 2/2′ were also observed as dominant on the shelves and slope of the Labrador Sea (Fragoso et al., 2018). Through a similar trait-based approach, Fragoso et al. (2018) found that these diatoms compared to the adjacent assemblage shared unique functional traits that enable them to thrive in these waters.

Resting spore formation is a strategy to overcome unfavourable conditions such as low light levels (McQuoid and Hobson, 1996), low temperatures (Durbin, 1978), as well as iron (Sugie and Kuma, 2008) or macronutrient limitations (Kuwata and Takahashi, 1990; Oku and Kamatani, 1995; Kuwata and Takahashi, 1999). Heavily silicified resting spores are also resistant to grazing (Kuwata and Tsuda, 2005) and may play an important role in seeding the seasonal diatom bloom (McQuoid and Hobson, 1996). The fact that the propensity to form resting spores is a functional trait characterizing the blooming assemblage 2/2′ could also explain (together with the differences in water masses and the pre-bloom nutrient inventory) why this assemblage did not develop at the ice edge of the stations located on the western side of the sampling area (stations 600, 604.5, 605, 519, 713 and 719). These stations are located over the deep abyssal plain (>2000 m), whereas most of the stations belonging to cluster 2/2′ were located over the shallower continental shelf and slope (<550 m, except for stations 312 and 707). Over the shelf and slope, resting spores lying on the seabed since the last bloom can be brought up to the surface more easily during winter convection, as opposed to the spores lying in the deepest part of the bay. These spores would germinate the following spring and form the inoculum for the spring bloom. In this study, several centric species were found to form resting spores, including *Thalassiosira antarctica var. borealis* and *Melosira arctica*. The highest formation of spores was observed at station 512, with an active sporulation event of *M. artica*, as shown by both cell counts and PDMPO staining. Although this station was not covered by the ice pack at the time of sampling, the sea ice had very recently melted (DOW50 = 3 days), which could explain the presence of *Melosira arctica* in the water column, a diatom known to grow meter-long filaments anchored on the underside of the sea ice (Boetius et al., 2013). In addition, st. 512 was characterized by the complete depletion down to detection limits of all nutrients (Si, N, P) at the surface, with the exception of NH_4 levels which remained high (0.23 μmol L^{-1}) and could indicate more intensive grazing activity. Hence, nutrient depletion together with grazing activity towards the end of the bloom would likely result in more widespread spore formation of centric species, and particularly of *M. arctica* which may be a strong contributor to both Si and C export to depth (Boetius et al., 2013).

The presence of cellular protuberances in the cluster 2/2′ assemblage such as setae in *Chaetoceros* spp. and long processes in *Thalassiosira* spp. may slow the gravitational settling of large and dense cells (Nguyen et al., 2011). However, another hypothesis has been proposed

for *Chaetoceros gelidus*. This species possesses long specialized setae which can join small chains together into larger colonies (Alldredge and Gotschalk, 1989), thus enabling the colony to sink faster and to reach deeper layers where more nutrients are available and where cells are less subject to photo-oxidative effects (Booth et al., 2002).

Ribbon-forming pennate species belonging to *Fragilariopsis* spp. and *Fossula arctica* were important contributors to both communities. Although identification at the species level was not always possible under the light microscope, SEM images (Figure S1) highlighted the importance of *Fragilariopsis cylindrus*. This species is known to be found in high abundances in sea ice as well as in the water column (Quillfeldt, 2004). Its success might be explained by its high degree of phenotypic plasticity (Petrou et al., 2010; Sackett et al., 2013). The recent sequencing of its whole genome also revealed a high percentage of highly divergent alleles (24.7%) that are differentially expressed across variable environmental conditions, notably genes involved in photosynthesis, light harvesting and photoprotection (Mock et al., 2017).

Hence, our trait-based analysis demonstrated that the diatoms associated with the core of the bloom possessed specific functional traits, which may enable them to thrive under extreme and rapidly changing environments such as melting sea ice. Functional traits can be linked to the ecological niches to derive generality and predictability on species biogeography. The combination of the traditional taxonomic approach (based on names of taxa) with functional trait analysis thus can be a powerful tool for predicting the influence of climate change on diatom species biogeography (Mcgill et al., 2006).

Conclusion

During the Green Edge expedition in central Baffin Bay, the development of the diatom bloom was studied in relation with the retreat of the ice pack. A late spring–early summer diatom bloom was well established in open waters and extended 20–30 km beneath the ice pack, following the alleviation of light limitation with the retreat of sea ice towards the Canadian coast. This diatom assemblage (cluster 2/2′) was strongly dominated by colonial fast-growing centric species (*Chaetoceros* spp. and *Thalassiosira* spp.) and ribbon-forming pennate species (*Fragilariopsis* spp./*Fossula arctica*), and was associated with high concentrations of Chl *a* and BSi, contributing on average to 22% of total POC (and up to 66%). This assemblage was found mostly over the shallow Greenland continental shelf and slope in Atlantic-influenced waters entering Baffin Bay from the south and flowing northwards along the Greenland coast. This development resulted in a near depletion of all nutrients at certain sites in surface waters, which probably induced the formation of resting spores of the colonial centric *Melosira arctica*. The diatoms composing this assemblage possessed functional traits that may enable them to thrive under these conditions such as the propensity to form large colonies and resting spores that may be exported rapidly to depth. The bloom is assumed to have lasted about 20 days, before being halted by nutrient limitation and increased grazing pressure, as suggested by pigment data. A second diatom assemblage (cluster 1/1′), composed mostly of solitary or colonial pennate species (*Pseudo-nitzschia* spp., *Ceratoneis closterium*, *Fragilariopsis* spp./*Fossula arctica*) was observed, mostly in western areas still covered by sea ice and/or more influenced by Pacific waters flowing down from the northern part of the Baffin Bay. This assemblage was associated with much less productive waters, with low biomass. It contributed on average only 3% of total POC, implying that other phytoplankton groups were dominating the bloom in these areas. Some extremely high abundances of *Phaeocystis* spp. were found to co-occur with this diatom assemblage at certain locations. Yet despite lower total Si production, this assemblage presented slightly higher specific Si uptake rates at stations located under the ice pack, probably reflecting early stages of the bloom not yet experiencing nutrient limitation.

In the context of climate change, we can expect that the predicted increase in the duration of the open water season will not directly affect the magnitude of the diatom bloom in central Baffin Bay, as the diatom development is already limited by nitrogen supply. However, with the earlier melting of the sea ice and alleviation of light limitation, the diatom bloom could occur earlier in the season. An earlier bloom would promote either trophic transfer along the food chain or carbon sinking, depending on a match or mismatch between secondary producers and the annual peak in primary production.

Data Accessibility Statement

All data are accessible at the Green Edge data base (http://www.obs-vlfr.fr/proof/php/GREENEDGE/greenedge.php) and will be made accessible after publication.

Supplemental files

The supplemental files for this article can be found as follows:

- **Table S1.** Linear measurements, biovolume, and carbon biomass of the taxa observed in Baffin Bay. DOI: https://doi.org/10.1525/elementa.382.s1
- **Table S2.** Functional trait data for the taxa observed in Baffin Bay. DOI: https://doi.org/10.1525/elementa.382.s1
- **Table S3.** Summary of the environmental and biological data at the 29 stations. DOI: https://doi.org/10.1525/elementa.382.s1
- **Table S4.** Diatoms observed in Baffin Bay during the Green Edge expedition. DOI: https://doi.org/10.1525/elementa.382.s1
- **Figure S1.** Selection of diatom species observed by scanning electron microscopy (SEM). DOI: https://doi.org/10.1525/elementa.382.s1
- **Figure S2.** T-S diagram for all of the stations. DOI: https://doi.org/10.1525/elementa.382.s1
- **Figure S3.** Vertical distribution of concentrations of chlorophyll a and nutrients (nitrate, orthosilicic acid, and phosphate) for transect T3. DOI: https://doi.org/10.1525/elementa.382.s1

- **Figure S4.** Integrated nutrient concentrations over the depth of the equivalent mixed layer (hBD). DOI: https://doi.org/10.1525/elementa.382.s1
- **Figure S5.** Potential limiting nutrients in rank order (most limiting first) based on nutrient ratios. DOI: https://doi.org/10.1525/elementa.382.s1
- **Figure S6.** Abundance of Phaeocystis spp. in surface waters and at the subsurface chlorophyll a maximum. DOI: https://doi.org/10.1525/elementa.382.s1
- **Figure S7.** Examples of actively silicifying diatoms labelled with the fluorescent dye PDMPO. DOI: https://doi.org/10.1525/elementa.382.s1
- **Figure S8.** Five-day composite images of satellite-derived surface chlorophyll a in Baffin Bay during April–August 2016. DOI: https://doi.org/10.1525/elementa.382.s1

Acknowledgements

The project is conducted under the scientific coordination of the Canada Excellence Research Chair on Remote sensing of Canada's new Arctic frontier and the CNRS & Université Laval Takuvik Joint International Laboratory (UMI3376).

We thank officers and crew of CCGS *Amundsen*, Marie-Hélène Forget and Joannie Ferland for organizing the fieldwork, and all other scientists and technicians involved in the Green Edge campaign for their contributions to fieldwork and data collection. They include in particular Pascal Guillot and the Amundsen Science Data team for the CTD data processing and quality control (UQAR-ISMER). Tonya Burgers and Brent Else kindly provided the shipboard PAR measurements. Sandrine Hillion performed the ^{32}Si incubation experiments. We thank I. Probert and D. Vaulot (Station Biologique de Roscoff, France) for access to their Phenom Pro Scanning Electron Microscope for species identification.

Funding information

The Green Edge project is funded by the following Canadian and French programs and agencies: the Network of Centres of Excellence ArcticNet, the Canada Foundation for Innovation (Amundsen Science), Canada's Excellence in Research Chair (CERC) program, ANR (Contract #111112), CNES (project #131425), French Arctic Initiative, Fondation Total, CSA, LEFE and IPEV (project #1164).

Competing interests

The authors have no competing interests to declare.

Author contributions

- Contributed to conception and design: AL, KL, BQ
- Contributed to acquisition of data: AL, BM, AL, JL, MP, JR, NG, PET
- Contributed to analysis and interpretation of data: AL, KL, BQ, JL
- Drafted and/or revised the article: AL, KL, BQ, BM, AL, MB, JR
- Approved the submitted version for publication: AL, KL, BQ, BM, AL, VC, MB, MP, JR, NG, PET

References

ACIA. 2005. Arctic climate impact assessment. Cambridge Univ. Press.

Alldredge, AL and **Gotschalk, CC.** 1989. Direct observations of the mass flocculation of diatom blooms: characteristics, settling velocities and formation of diatom aggregates. *Deep Sea Res* **36**(2): 159–171. DOI: https://doi.org/10.1016/0198-0149(89)90131-3

Antajan, E, Chrétiennot-Dinet, MJ, Leblanc, C, Daro, MH and **Lancelot, C.** 2004. 19′-hexanoyloxyfucoxanthin may not be the appropriate pigment to trace occurrence and fate of *Phaeocystis*: the case of *P. globosa* in Belgian coastal waters. *J Sea Res* **52**(3): 165–177. DOI: https://doi.org/10.1016/j.seares.2004.02.003

Ardyna, M, Babin, M, Gosselin, M, Devred, E, Rainville, L and **Tremblay, JÉ.** 2014. Recent Arctic Ocean sea ice loss triggers novel fall phytoplankton blooms. *Geophys Res Lett* **41**(17): 6207–6212. DOI: https://doi.org/10.1002/2014GL061047

Arrigo, KR and **van Dijken, GL.** 2011. Secular trends in Arctic Ocean net primary production. *J Geophys Res* **116**(C9). DOI: https://doi.org/10.1029/2011JC007151

Arrigo, KR, van Dijken, GL and **Pabi, S.** 2008. Impact of a shrinking Arctic ice cover on marine primary production. *Geophys Res Lett* **35**(19). DOI: https://doi.org/10.1029/2008GL035028

Arrigo, KR, Perovich, DK, Pickart, RS, Brown, ZW, van Dijken, GL, Lowry, KE, Mills, MM, Palmer, MA, Balch, WM, Bahr, F, Bates, NR, Benitez-Nelson, C, Bowler, B, Brownlee, E, Ehn, JK, Frey, KE, Garley, R, Laney, SR, Lubelczyk, L, Mathis, J, Matsuoka, A, Mitchell, BG, Moore, GWK, Ortega-Retuerta, E, Pal, S, Polashenski, CM, Reynolds, RA, Schieber, B, Sosik, HM, Stephens, M and **Swift, JH.** 2012. Massive phytoplankton blooms under Arctic sea ice. *Science* **336**(6087). DOI: https://doi.org/10.1126/science.1215065

Arrigo, KR, Perovich, DK, Pickart, RS, Brown, ZW, van Dijken, GL, Lowry, KE, Mills, MM, Palmer, MA, Balch, WM, Bates, NR, Benitez-Nelson, CR, Brownlee, E, Frey, KE, Laney, SR, Mathis, J, Matsuoka, A, Greg Mitchell, B, Moore, GWK, Reynolds, RA, Sosik, HM and **Swift, JH.** 2014. Phytoplankton blooms beneath the sea ice in the Chukchi sea. *Deep Sea Res Pt II* **105**: 1–16. DOI: https://doi.org/10.1016/j.dsr2.2014.03.018

Assmy, P, Fernández-Méndez, M, Duarte, P, Meyer, A, Randelhoff, A, Mundy, CJ, Olsen, LM, Kauko, HM, Bailey, A, Chierici, M, Cohen, L, Doulgeris, AP, Ehn, JK, Fransson, A, Gerland, S, Hop, H, Hudson, SR, Hughes, N, Itkin, P, Johnsen, G, King, JA, Koch, BP, Koenig, Z, Kwasniewski, S, Laney, SR, Nicolaus, M, Pavlov, AK, Polashenski, CM, Provost, C, Rösel, A, Sandbu, M, Spreen, G, Smedsrud, LH, Sundfjord, A, Taskjelle, T, Tatarek, A, Wiktor, J, Wagner, PM, Wold, A, Steen, H and **Granskog, MA.** 2017. Leads in Arctic pack ice enable early phytoplankton blooms below

snow-covered sea ice. *Sci Rep* **7**: 40850. DOI: https://doi.org/10.1038/srep40850

Baines, SB, Twining, BS, Brzezinski, MA, Nelson, DM and **Fisher, NS.** 2010. Causes and biogeochemical implications of regional differences in silicification of marine diatoms. *Glob Biogeochem Cycles* **24**(4). DOI: https://doi.org/10.1029/2010GB003856

Beitsch, A, Kaleschke, L and **Kern, S.** 2014. Investigating high-resolution AMSR2 sea ice concentrations during the February 2013 fracture event in the Beaufort Sea. *Remote Sens* **6**(5): 3841–3856. DOI: https://doi.org/10.3390/rs6053841

Bélanger, S, Babin, M and **Tremblay, JÉ.** 2013. Increasing cloudiness in Arctic damps the increase in phytoplankton primary production due to sea ice receding. *Biogeosciences* **10**(6): 4087–4101. DOI: https://doi.org/10.5194/bg-10-4087-2013

Boetius, A, Albrecht, S, Bakker, K, Bienhold, C, Felden, J, Fernandez-Mendez, M, Hendricks, S, Katlein, C, Lalande, C, Krumpen, T, Nicolaus, M, Peeken, I, Rabe, B, Rogacheva, A, Rybakova, E, Somavilla, R, Wenzhofer, F and **RV Polarstern ARK27-3-Shipboard Science Party.** 2013. Export of algal biomass from the melting Arctic sea ice. *Science* **339**(6126): 1430–1432. DOI: https://doi.org/10.1126/science.1231346

Booth, BC, Larouche, P, Bélanger, S, Klein, B, Amiel, D and **Mei, ZP.** 2002. Dynamics of *Chaetoceros socialis* blooms in the North Water. *Deep Sea Res Pt II* **49**(22–23): 5003–5025. DOI: https://doi.org/10.1016/S0967-0645(02)00175-3

Brzezinski, MA. 1985. The Si:C:N ratio of marine diatoms: interspecific variability and the effect of some environmental variables. *J Phycol* **21**(3): 347–357. DOI: https://doi.org/10.1111/j.0022-3646.1985.00347.x

Brzezinski, MA and **Phillips, DR.** 1997. Evaluation of ^{32}Si as a tracer for measuring silica production rates in marine waters. *Limnol Oceanogr* **42**(5): 856–865. DOI: https://doi.org/10.4319/lo.1997.42.5.0856

BS EN 16695. 2015. Water quality. Guidance on the estimation of phytoplankton biovolume. Available at https://shop.bsigroup.com/ProductDetail/?pid=000000000030291480.

Chiswell, SM, Calil, PHR and **Boyd, PW.** 2015. Spring blooms and annual cycles of phytoplankton: a unified perspective. *J Plankton Res* **37**(3): 500–508. DOI: https://doi.org/10.1093/plankt/fbv021

Comiso, JC. 2002. A rapidly declining perennial sea ice cover in the Arctic. *Geophys Res Lett* **29**(20). DOI: https://doi.org/10.1029/2002GL015650

Cornet-Barthaux, V, Armand, L and **Quéguiner, B.** 2007. Biovolume and biomass estimates of key diatoms in the Southern Ocean. *Aquat Microb Ecol* **48**: 295–308. DOI: https://doi.org/10.3354/ame048295

Degerlund, M and **Eilertsen, HC.** 2010. Main species characteristics of phytoplankton spring blooms in NE Atlantic and Arctic waters (68–80°N). *Estuaries Coasts* **33**(2): 242–269. DOI: https://doi.org/10.1007/s12237-009-9167-7

Durbin, EG. 1978. Aspects of the biology of resting spores of *Thalassiosira nordenskioeldii* and *Detonula confervacea*. *Mar Biol* **45**(1): 31–37. DOI: https://doi.org/10.1007/BF00388975

Durkin, C, Marchetti, A, Bender, S, Truong, T, Morales, R, Mock, T and **Armbrust, E.** 2012. Frustule-related gene transcription and the influence of diatom community composition on silica precipitation in an iron-limited environment. *Limnol Ocean* **57**(6): 1619–1633. DOI: https://doi.org/10.4319/lo.2012.57.6.1619

Fragoso, GM, Poulton, AJ, Yashayaev, IM, Head, EJH, Johnsen, G and **Purdie, DA.** 2018. Diatom biogeography from the Labrador Sea revealed through a trait-based approach. *Front Mar Sci* **5**. DOI: https://doi.org/10.3389/fmars.2018.00297

Goldman, JC. 1993. Potential role of large oceanic diatoms in new primary production. *Deep Sea Res* **40**(1): 159–168. DOI: https://doi.org/10.1016/0967-0637(93)90059-C

Grasshoff, K, Kremling, K and **Ehrhardt, M.** 2009. *Methods of Seawater Analysis*. John Wiley & Sons.

Hegseth, EN and **Sundfjord, A.** 2008. Intrusion and blooming of Atlantic phytoplankton species in the high Arctic. *J Mar Syst* **74**(1–2): 108–119. DOI: https://doi.org/10.1016/j.jmarsys.2007.11.011

Hodal, H, Falk-Petersen, S, Hop, H, Kristiansen, S and **Reigstad, M.** 2012. Spring bloom dynamics in Kongsfjorden, Svalbard: nutrients, phytoplankton, protozoans and primary production. *Polar Biol* **35**(2): 191–203. DOI: https://doi.org/10.1007/s00300-011-1053-7

IPCC. 2007. Climate change 2007: the physical science basis; contribution of Working Group I to the Fourth Assessment Report of the Intergovernmental Panel on Climate Change. Cambridge University Press.

Jakobsen, H and **Tang, K.** 2002. Effects of protozoan grazing on colony formation in *Phaeocystis globosa* (Prymnesiophyceae) and the potential costs and benefits. *Aquat Microb Ecol* **27**: 261–273. DOI: https://doi.org/10.3354/ame027261

Jones, EP, Anderson, LG and **Swift, JH.** 1998. Distribution of Atlantic and Pacific waters in the upper Arctic Ocean: Implications for circulation. *Geophys Res Lett* **25**(6): 765–768. DOI: https://doi.org/10.1029/98GL00464

Kahru, M, Brotas, V, Manzano-Sarabia, M and **Mitchell, BG.** 2011. Are phytoplankton blooms occurring earlier in the Arctic? *Glob Change Biol* **17**(4): 1733–1739. DOI: https://doi.org/10.1111/j.1365-2486.2010.02312.x

Kuwata, A and **Takahashi, M.** 1990. Life-form population responses of a marine planktonic diatom, *Chaetoceros pseudocurvisetus*, to oligotrophication in regionally upwelled water. *Mar Biol* **107**(3): 503–512. DOI: https://doi.org/10.1007/BF01313435

Kuwata, A and **Takahashi, M.** 1999. Survival and recovery of resting spores and resting cells of the

marine planktonic diatom *Chaetoceros pseudocurvisetus* under fluctuating nitrate conditions. *Mar Biol* **134**(3): 471–478. DOI: https://doi.org/10.1007/s002270050563

Kuwata, A and **Tsuda, A.** 2005. Selection and viability after ingestion of vegetative cells, resting spores and resting cells of the marine diatom, *Chaetoceros pseudocurvisetus*, by two copepods. *J Exp Mar Biol Ecol* **322**(2): 143–151. DOI: https://doi.org/10.1016/j.jembe.2005.02.013

Kwok, R, Cunningham, GF, Wensnahan, M, Rigor, I, Zwally, HJ and **Yi, D.** 2009. Thinning and volume loss of the Arctic Ocean sea ice cover: 2003–2008. *J Geophys Res* **114**(C7). DOI: https://doi.org/10.1029/2009JC005312

Laney, SR and **Sosik, HM.** 2014. Phytoplankton assemblage structure in and around a massive under-ice bloom in the Chukchi Sea. *Deep Sea Res Pt II* **105**: 30–41. DOI: https://doi.org/10.1016/j.dsr2.2014.03.012

Leblanc, K, Arístegui, J, Armand, L, Assmy, P, Beker, B, Bode, A, Breton, E, Cornet, V, Gibson, J, Gosselin, M-P, Kopczynska, E, Marshall, H, Peloquin, J, Piontkovski, S, Poulton, A, Quéguiner, B, Schiebel, R, Shipe, R, Stefels, J, Leeuwe, M, Varela, M, Widdicombe, C and **Yallop, M.** 2012. A global diatom database – abundance, biovolume and biomass in the world ocean. *Earth Syst Sci Data* **4**(1): 149–165. DOI: https://doi.org/10.5194/essd-4-149-2012

Leblanc, K and **Hutchins, DA.** 2005. New applications of a biogenic silica deposition fluorophore in the study of oceanic diatoms. *Limnol Oceanogr Methods* **3**(10): 462–476. DOI: https://doi.org/10.4319/lom.2005.3.462

Legendre, P and **Legendre, L.** 2012. *Numerical Ecology*. 3. Engl. ed. Amsterdam: Elsevier. (Developments in environmental modelling; Vol. 24).

Letelier, RM, Karl, DM, Abbott, MR and **Bidigare, RR.** 2004. *Light driven seasonal patterns of chlorophyll and nitrate in the lower euphotic zone of the North Pacific Subtropical Gyre* **49**(2): 508–519. DOI: https://doi.org/10.4319/lo.2004.49.2.0508

Lind, S, Ingvaldsen, RB and **Furevik, T.** 2018. Arctic warming hotspot in the northern Barents Sea linked to declining sea-ice import. *Nat Clim Change* **8**(7): 634–639. DOI: https://doi.org/10.1038/s41558-018-0205-y

Litchman, E and **Klausmeier, CA.** 2008. Trait-based community ecology of phytoplankton. *Annu Rev Ecol Evol Syst* **39**(1): 615–639. DOI: https://doi.org/10.1146/annurev.ecolsys.39.110707.173549

Litchman, E, Klausmeier, CA, Schofield, OM and **Falkowski, PG.** 2007. The role of functional traits and trade-offs in structuring phytoplankton communities: scaling from cellular to ecosystem level. *Ecol Lett* **10**(12): 1170–1181. DOI: https://doi.org/10.1111/j.1461-0248.2007.01117.x

Lovejoy, C, Legendre, L, Martineau, MJ, Bâcle, J and **Quillfeldt, CH von.** 2002. Distribution of phytoplankton and other protists in the North Water. *Deep Sea Res Pt II* **49**(22–23): 5027–5047. DOI: https://doi.org/10.1016/S0967-0645(02)00176-5

Maslanik, J, Stroeve, J, Fowler, C and **Emery, W.** 2011. Distribution and trends in Arctic sea ice age through spring 2011. *Geophys Res Lett* **38**(13). DOI: https://doi.org/10.1029/2011GL047735

Massicotte, P, Amiraux, R, Amyot, M-P, Archambault, P, Ardyna, M, Arnaud, L, Artigue, L, Aubry, C, Ayotte, P, Bécu, G, Bélanger, S, Benner, R, Bittig, HC, Bricaud, A, Brossier, É, Bruyant, F, Chauvaud, L, Christiansen-Stowe, D, Claustre, H, Cornet-Barthaux, V, Coupel, P, Cox, C, Delaforge, A, Dezutter, T, Dimier, C, Dominé, F, Dufour, F, Dufresne, C, Dumont, D, Ehn, J, Else, B, Ferland, J, Forget, M-H, Fortier, L, Galí, M, Galindo, V, Gallinari, M, Garcia, N, Gérikas-Ribeiro, C, Gourdal, M, Gourvil, P, Goyens, C, Grondin, P-L, Guillot, P, Guilmette, C, Houssais, M-N, Joux, F, Lacour, L, Lacour, T, Lafond, A, Lagunas, J, Lalande, C, Laliberté, J, Lambert-Girard, S, Larivière, J, Lavaud, J, Le Gall, F, LeBaron, A, Leblanc, K, Legras, J, Lemire, M, Levasseur, M, Leymarie, E, Leynaert, A, Lopes dos Santos, A, Lourenço, A, Mah, D, Marec, C, Marie, D, Martin, N, Marty, C, Marty, S, Massé, G, Matsuoka, A, Matthes, L, Moriceau, B, Muller, P-E, Mundy, CJ, Neukermans, G, Oziel, L, Panagiotopoulos, C, Pangazi, J-J, Picard, G, Picheral, M, Pinczon du Sel, F, Pogorzelec, N, Probert, I, Queguiner, B, Raimbault, P, Ras, J, Rehm, E, Reimer, E, Rontani, J-F, Rysgaard, S, Saint-Béat, B, Sampei, M, Sansoulet, J, Schmidt, S, Sempéré, R, Sévigny, C, Shen, Y, Tragin, M, Tremblay, J-É, Vaulot, D, Verin, G, Vivier, F, Vladoiu, A, Whitehead, J and **Babin, M.** 2019. Green Edge ice camp campaigns: understanding the processes controlling the under-ice Arctic phytoplankton spring bloom. *Earth Syst Sci Data Discuss*, 1–42 (in press). DOI: https://doi.org/10.5194/essd-2019-160

Mcgill, B, Enquist, B, Weiher, E and **Westoby, M.** 2006. Rebuilding community ecology from functional traits. *Trends Ecol Evol* **21**(4): 178–185. DOI: https://doi.org/10.1016/j.tree.2006.02.002

McNair, HM, Brzezinski, MA and **Krause, JW.** 2015. Quantifying diatom silicification with the fluorescent dye, PDMPO. *Limnol Oceanogr Methods* **13**(10): 587–599. DOI: https://doi.org/10.1002/lom3.10049

McNair, HM, Brzezinski, MA, Till, CP and **Krause, JW.** 2018. Taxon-specific contributions to silica production in natural diatom assemblages. *Limnol Oceanogr* **63**(3): 1056–1075. DOI: https://doi.org/10.1002/lno.10754

McQuoid, MR and **Hobson, LA.** 1996. Diatom resting stages. *J Phycol* **32**(6): 889–902. DOI: https://doi.org/10.1111/j.0022-3646.1996.00889.x

Metfies, K, von Appen, WJ, Kilias, E, Nicolaus, A and **Nöthig, EM.** 2016. Biogeography and photosynthetic biomass of Arctic marine pico-eukaroytes during summer of the record sea ice minimum 2012. In: Vopel, KC (ed.), *PLOS ONE* **11**(2): e0148512. DOI: https://doi.org/10.1371/journal.pone.0148512

Mock, T, Otillar, RP, Strauss, J, McMullan, M, Paajanen, P, Schmutz, J, Salamov, A, Sanges, R, Toseland, A, Ward, BJ, Allen, AE, Dupont, CL, Frickenhaus, S, Maumus, F, Veluchamy, A, Wu, T, Barry, KW, Falciatore, A, Ferrante, MI, Fortunato, AE, Glöckner, G, Gruber, A, Hipkin, R, Janech, MG, Kroth, PG, Leese, F, Lindquist, EA, Lyon, BR, Martin, J, Mayer, C, Parker, M, Quesneville, H, Raymond, JA, Uhlig, C, Valas, RE, Valentin, KU, Worden, AZ, Armbrust, EV, Clark, MD, Bowler, C, Green, BR, Moulton, V, van Oosterhout, C and **Grigoriev, IV.** 2017. Evolutionary genomics of the cold-adapted diatom *Fragilariopsis cylindrus*. *Nature* **541**(7638): 536–540. DOI: https://doi.org/10.1038/nature20803

Mundy, CJ, Barber, DG and **Michel, C.** 2005. Variability of snow and ice thermal, physical and optical properties pertinent to sea ice algae biomass during spring. *J Mar Syst* **58**(3–4): 107–120. DOI: https://doi.org/10.1016/j.jmarsys.2005.07.003

Mundy, CJ, Ehn, JK, Barber, DG and **Michel, C.** 2007. Influence of snow cover and algae on the spectral dependence of transmitted irradiance through Arctic landfast first-year sea ice. *J Geophys Res* **112**(C3). DOI: https://doi.org/10.1029/2006JC003683

Mundy, CJ, Gosselin, M, Gratton, Y, Brown, K, Galindo, V, Campbell, K, Levasseur, M, Barber, D, Papakyriakou, T and **Bélanger, S.** 2014. Role of environmental factors on phytoplankton bloom initiation under landfast sea ice in Resolute Passage, Canada. *Mar Ecol Prog Ser* **497**: 39–49. DOI: https://doi.org/10.3354/meps10587

Nelson, DM, Smith, WO, Muench, RD, Gordon, LI, Sullivan, CW and **Husby, DM.** 1989. Particulate matter and nutrient distributions in the ice-edge zone of the Weddell Sea: relationship to hydrography during late summer. *Deep Sea Res* **36**(2): 191–209. DOI: https://doi.org/10.1016/0198-0149(89)90133-7

Nguyen, H, Karp-Boss, L, Jumars, PA and **Fauci, L.** 2011. Hydrodynamic effects of spines: A different spin. *Limnol Oceanogr Fluids Environ* **1**(1): 110–119. DOI: https://doi.org/10.1215/21573698-1303444

Nöthig, E-M, Bracher, A, Engel, A, Metfies, K, Niehoff, B, Peeken, I, Bauerfeind, E, Cherkasheva, A, Gäbler-Schwarz, S, Hardge, K, Kilias, E, Kraft, A, Mebrahtom Kidane, Y, Lalande, C, Piontek, J, Thomisch, K and **Wurst, M.** 2015. Summertime plankton ecology in Fram Strait—a compilation of long- and short-term observations. *Polar Res* **34**(1): 23349. DOI: https://doi.org/10.3402/polar.v34.23349

Oku, O and **Kamatani, A.** 1995. Resting spore formation and phosphorus composition of the marine diatom *Chaetoceros pseudocurvisetus* under various nutrient conditions. *Mar Biol* **123**(2): 393–399. DOI: https://doi.org/10.1007/BF00353630

Paasche, E. 1973. Silicon and the ecology of marine plankton diatoms. I. *Thalassiosira pseudonana* (*Cyclotella nana*) grown in a chemostat with silicate as limiting nutrient. *Mar Biol* **19**(2): 117–126. DOI: https://doi.org/10.1007/BF00353582

Pabi, S, van Dijken, GL and **Arrigo, KR.** 2008. Primary production in the Arctic Ocean, 1998–2006. *J Geophys Res* **113**(C8). DOI: https://doi.org/10.1029/2007JC004578

Perrette, M, Yool, A, Quartly, GD and **Popova, EE.** 2011. Near-ubiquity of ice-edge blooms in the Arctic. *Biogeosciences* **8**(2): 515–524. DOI: https://doi.org/10.5194/bg-8-515-2011

Petrou, K, Hill, R, Brown, CM, Campbell, DA, Doblin, MA and **Ralph, PJ.** 2010. Rapid photoprotection in sea-ice diatoms from the East Antarctic pack ice. *Limnol Oceanogr* **55**(3): 1400–1407. DOI: https://doi.org/10.4319/lo.2010.55.3.1400

Poulin, M, Daugbjerg, N, Gradinger, R, Ilyash, L, Ratkova, T and **Quillfeldt, CH von.** 2011. The pan-Arctic biodiversity of marine pelagic and sea-ice unicellular eukaryotes: a first-attempt assessment. *Mar Biodivers* **41**(1): 13–28. DOI: https://doi.org/10.1007/s12526-010-0058-8

Quillfeldt, CH von. 2000. Common diatom species in Arctic spring blooms: Their distribution and abundance. *Bot Mar* **43**(6). DOI: https://doi.org/10.1515/BOT.2000.050

Quillfeldt, CH von. 2001. Identification of some easily confused common diatom species in Arctic spring blooms. *Bot Mar* **44**(4). DOI: https://doi.org/10.1515/BOT.2001.048

Quillfeldt, CH von. 2004. The diatom *Fragilariopsis cylindrus* and its potential as an indicator species for cold water rather than for sea ice. *Vie Milieu* **54**: 137–143.

Ragueneau, O and **Tréguer, P.** 1994. Determination of biogenic silica in coastal waters: applicability and limits of the alkaline digestion method. *Mar Chem* **45**(1–2): 43–51. DOI: https://doi.org/10.1016/0304-4203(94)90090-6

Randelhoff, A, Fer, I and **Sundfjord, A.** 2017. Turbulent upper-ocean mixing affected by meltwater layers during Arctic summer. *J Phys Oceanogr* **47**(4): 835–853. DOI: https://doi.org/10.1175/JPO-D-16-0200.1

Randelhoff, A, Oziel, L, Massicotte, P, Bécu, G, Galí, M, Lacour, L, Dumont, D, Vladoiu, A, Marec, C, Bruyant, F, Houssais, M-N, Tremblay, J-É, Deslongchamps, G and **Babin, M.** 2019. The evolution of light and vertical mixing across a phytoplankton ice-edge bloom. *Elem Sci Anth* **7**(1): 20. DOI: https://doi.org/10.1525/elementa.357

Ras, J, Claustre, H and **Uitz, J.** 2008. Spatial variability of phytoplankton pigment distributions in the

Subtropical South Pacific Ocean: comparison between in situ and predicted data. *Biogeosciences* **5**(2): 353–369. DOI: https://doi.org/10.5194/bg-5-353-2008

Redfield, AC, Ketchum, BH and **Richards, FA.** 1963. The influence of organisms on the composition of seawater. *The Sea*, 26–77. New York.

Reid, PC, Johns, DG, Edwards, M, Starr, M, Poulin, M and **Snoeijs, P.** 2007. A biological consequence of reducing Arctic ice cover: arrival of the Pacific diatom *Neodenticula seminae* in the North Atlantic for the first time in 800,000 years. *Glob Change Biol* **13**(9): 1910–1921. DOI: https://doi.org/10.1111/j.1365-2486.2007.01413.x

Ricchiazzi, P, Yang, S, Gautier, C and **Sowle, D.** 1998. SBDART: A research and teaching software tool for plane-parallel radiative transfer in the Earth's atmosphere. *Bull Am Meteorol Soc* **79**(10): 2101–2114. DOI: https://doi.org/10.1175/1520-0477(1998)079<2101:SARATS>2.0.CO;2

Rysgaard, S, Nielsen, TG and **Hansen, BW.** 1999. Seasonal variation in nutrients, pelagic primary production and grazing in a high-Arctic coastal marine ecosystem, Young Sound, Northeast Greenland. *Mar Ecol Prog Ser* **179**: 13–25. DOI: https://doi.org/10.3354/meps179013

Sackett, O, Petrou, K, Reedy, B, De Grazia, A, Hill, R, Doblin, M, Beardall, J, Ralph, P and **Heraud, P.** 2013. Phenotypic plasticity of Southern Ocean diatoms: Key to success in the sea ice habitat? *PLoS ONE* **8**(11). DOI: https://doi.org/10.1371/journal.pone.0081185

Sakshaug, E. 2004. Primary and secondary production in the Arctic seas. In: Stein, R and MacDonald, RW (eds.), *The Organic Carbon Cycle in the Arctic Ocean*, 57–81. Berlin, Heidelberg: Springer Berlin Heidelberg. DOI: https://doi.org/10.1007/978-3-642-18912-8_3

Sakshaug, E and **Skjoldal, HR.** 1989. Life at the ice edge. *Ambio* **18**(1): 8.

Smayda, TJ. 1978. From phytoplankton to biomass. In: Sournia, A (ed.), *Phytoplankton Manual*, 273–279. Repr. Paris: Unesco.

Smith, WO and **Nelson, DM.** 1985. Phytoplankton bloom produced by a receding tce edge in the Ross Sea: Spatial Coherence with the Density Field. *Science* **227**(4683): 163–166. DOI: https://doi.org/10.1126/science.227.4683.163

Steinacher, M, Joos, F, Frolicher, TL, Bopp, L, Cadule, P, Cocco, V, Doney, SC, Gehlen, M, Lindsay, K and **Moore, JK.** 2010. Projected 21st century decrease in marine productivity: a multi-model analysis. *Biogeosciences* **7**(3). DOI: https://doi.org/10.5194/bg-7-979-2010

Stroeve, J, Holland, MM, Meier, W, Scambos, T and **Serreze, M.** 2007. Arctic sea ice decline: Faster than forecast. *Geophys Res Lett* **34**(9). DOI: https://doi.org/10.1029/2007GL029703

Stuart, V, Sathyendranath, S, Head, E, Platt, T, Irwin, B and **Maass, H.** 2000. Bio-optical characteristics of diatom and prymnesiophyte populations in the Labrador Sea. *Mar Ecol Prog Ser* **201**: 91–106. DOI: https://doi.org/10.3354/meps201091

Sugie, K and **Kuma, K.** 2008. Resting spore formation in the marine diatom *Thalassiosira nordenskioeldii* under iron- and nitrogen-limited conditions. *J Plankton Res* **30**(11): 1245–1255. DOI: https://doi.org/10.1093/plankt/fbn080

Tang, CCL, Ross, CK, Yao, T, Petrie, B, DeTracey, BM and **Dunlap, E.** 2004. The circulation, water masses and sea-ice of Baffin Bay. *Prog Oceanogr* **63**(4): 183–228. DOI: https://doi.org/10.1016/j.pocean.2004.09.005

Tréguer, P, Lindner, L, van Bennekom, AJ, Leynaert, A, Panouse, M and **Jacques, G.** 1991. Production of biogenic silica in the Weddell-Scotia Seas measured with ^{32}Si. *Limnol Oceanogr* **36**(6): 1217–1227. DOI: https://doi.org/10.4319/lo.1991.36.6.1217

Tremblay, J-É. 2002. Impact of the large-scale Arctic circulation and the North Water Polynya on nutrient inventories in Baffin Bay. *J Geophys Res* **107**(C8). DOI: https://doi.org/10.1029/2000JC000595

Tremblay, J-É and **Gagnon, J.** 2009. The effects of irradiance and nutrient supply on the productivity of Arctic waters: a perspective on climate change. In: Nihoul, JCJ and Kostianoy, AG (eds.), *Influence of Climate Change on the Changing Arctic and Sub-Arctic Conditions*, 73–93. Dordrecht: Springer Netherlands. DOI: https://doi.org/10.1007/978-1-4020-9460-6_7

Tungaraza, C, Rousseau, V, Brion, N, Lancelot, C, Gichuki, J, Baeyens, W and **Goeyens, L.** 2003. Contrasting nitrogen uptake by diatom and *Phaeocystis*-dominated phytoplankton assemblages in the North Sea. *J Exp Mar Biol Ecol* **292**(1): 19–41. DOI: https://doi.org/10.1016/S0022-0981(03)00145-X

Utermöhl, H. 1931. Neue Wege in der quantitativen Erfassung des Plankton. (Mit besonderer Berücksichtigung des Ultraplanktons.): Mit 4 Abbildungen im Text. *SIL Proc 1922–2010* **5**(2): 567–596. DOI: https://doi.org/10.1080/03680770.1931.11898492

Vancoppenolle, M, Bopp, L, Madec, G, Dunne, J, Ilyina, T, Halloran, PR and **Steiner, N.** 2013. Future Arctic Ocean primary productivity from CMIP5 simulations: Uncertain outcome, but consistent mechanisms. *Glob Biogeochem Cycles* **27**(3): 605–619. DOI: https://doi.org/10.1002/gbc.20055

Wang, M and **Overland, JE.** 2009. A sea ice free summer Arctic within 30 years? *Geophys Res Lett* **36**(7). DOI: https://doi.org/10.1029/2009GL037820

Wang, Q, Wekerle, C, Danilov, S, Koldunov, N, Sidorenko, D, Sein, D, Rabe, B and **Jung, T.** 2018. Arctic sea ice decline significantly contributed to the unprecedented liquid freshwater accumulation in the Beaufort Gyre of the Arctic Ocean. *Geophys Res Lett* **45**(10): 4956–4964. DOI: https://doi.org/10.1029/2018GL077901

Ward, JH. 1963. Hierarchical grouping to optimize an objective function. *J Am Stat Assoc* **58**(301): 236–244. DOI: https://doi.org/10.1080/01621459.1963.10500845

Wassmann, P, Carroll, J and **Bellerby, RGJ.** 2008. Carbon flux and ecosystem feedback in the northern Barents Sea in an era of climate change: An introduction. *Deep Sea Res Pt II* **55**(20–21): 2143–2153. DOI: https://doi.org/10.1016/j.dsr2.2008.05.025

Wassmann, P, Duarte, CM, Agustí, S and **Sejr, MK.** 2011. Footprints of climate change in the Arctic marine ecosystem. *Glob Change Biol* **17**(2): 1235–1249. DOI: https://doi.org/10.1111/j.1365-2486.2010.02311.x

Wassmann, P, Ratkova, T, Andreassen, I, Vernet, M, Pedersen, G and **Rey, F.** 1999. Spring bloom development in the marginal ice zone and the central Barents Sea. *Mar Ecol* **20**(3–4): 321–346. DOI: https://doi.org/10.1046/j.1439-0485.1999.2034081.x

How to cite this article: Lafond, A, Leblanc, K, Quéguiner, B, Moriceau, B, Leynaert, A, Cornet, V, Legras, J, Ras, J, Parenteau, M, Garcia, N, Babin, M and Tremblay, J-É. 2019. Late spring bloom development of pelagic diatoms in Baffin Bay. *Elem Sci Anth,* 7: 44. DOI: https://doi.org/10.1525/elementa.382

Domain Editor-in-Chief: Jody W. Deming, School of Oceanography, University of Washington, US

Associate Editor: Christine Michel, Fisheries and Oceans Canada, Freshwater Institute, CA

Knowledge Domain: Ocean Science

Part of an *Elementa* Special Feature: Green Edge

Submitted: 04 February 2019 **Accepted:** 20 October 2019 **Published:** 13 November 2019

ELEMENTA Science of the Anthropocene

Elem Sci Anth is a peer-reviewed open access journal published by University of California Press.

OPEN ACCESS